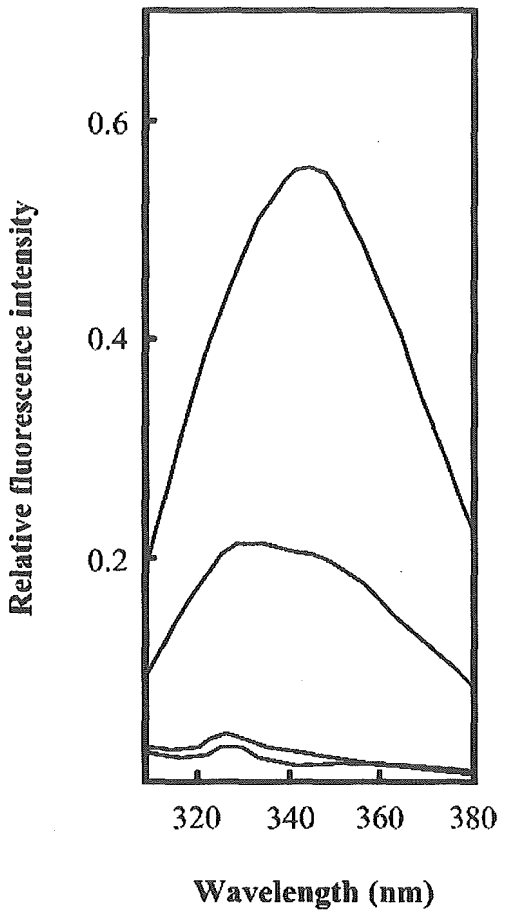

Fig. 2. Intrinsic fluorescence spectra of rHSA and individual domains. The protein concentration was 6 μM in 67 mM phosphate buffer (pH 7.4 and 25°C). From top to bottom, spectra for rHSA, domain II, domain III, and domain I.

buffer (pH 7.4), and a similar difference in activity was observed for domain II. However, this pattern of activity was not observed for the other two domains.

In order to confirm the involvement of domain II in the enolase-like activity of HSA, the enolase-like activity of rHSA (5 μM) for DHT (2 μM, 0.4 μCi) was measured in the presence of warfarin or ketoprofen (20 μM). No inhibition was observed in the presence of ketoprofen at pH 7.4 or 9.4. In contrast, in the presence of warfarin, a decrease in activity

Table II. Binding of Ketoprofen and DNSS to rHSA and Individual Domains

HSA	Percentage bound (%)	
	Ketoprofen	DNSS
rHSA	80.17 ± 6.73	62.43 ± 5.38
Domain I	6.07 ± 3.95[a,b]	4.21 ± 2.90[a,b]
Domain II	4.58 ± 1.61[a,b]	7.02 ± 2.87[a,b]
Domain III	64.00 ± 5.83[a]	38.92 ± 7.78[a]

The sample solutions contained 2.5 μM ketoprofen or DNSS and 5 μM rHSA or individual domains in 67 mM phosphate buffer (pH 7.4 and 25°C). All values are mean ± SD (n = 3 to 5).
[a] $p < 0.01$ vs. rHSA.
[b] $p < 0.01$ vs. domain III.

Table III. Hydrolysis Rate Constants (k_{obs}) for *p*-Nitrophenyl Acetate

HSA	k_{obs} ($s \times 10^{-3}$)
rHSA	7.13 ± 0.90
Domain I	1.73 ± 0.65[a]
Domain II	ND
Domain III	3.18 ± 0.83[a,b]

The reaction mixtures contained 5 μM *p*-nitrophenyl acetate and 20 μM rHSA or individual domains in 67 mM phosphate buffer (pH 7.4 and 25°C). All values are mean ± SD (n = 5 to 7). ND, not detectable.
[a] $p < 0.01$ vs. rHSA.
[b] $p < 0.01$ vs. domain I.

of about 35% was observed at pH 7.4, whereas no significant inhibition was observed at pH 9.4 (data not shown). These results suggest that the active site in site I is functional at pH 7.4, and that a new site different from site I is formed in domain II at pH 9.4, a process which is thought to be influenced by fragmentation.

Antioxidant Activity of the Recombinant HSA Domains

We examined the ability of each domain to inhibit the oxidation of DRD by H_2O_2. The RD generated by oxidation was used as an indicator of antioxidant activity (25). Figure 3 shows the capacity of rHSA and individual domains to quench DRD oxidation by H_2O_2. Domains II and III showed a weak inhibitory effect compared with rHSA, but the quenching capacity of domain I was comparable to that of rHSA.

In Vivo Studies

To evaluate whether fragmentation of domains affects the biologic fate of rHSA, we measured uptake clearance of rHSA and the corresponding domain proteins in mice (Table V). There was about a 50-fold difference in total clearance between rHSA and individual domains. However, there was no significant difference in total clearance among the domains. The three domains were mainly distributed in the kidney. However, domain III was found at slightly higher levels than other domains in the liver.

Table IV. Enolase-like Activity of rHSA and Individual Domains in Two Different Buffer Solutions

HSA	Phosphate buffer pH 7.4 (CPM)	Carbonate buffer pH 9.2 (CPM)
rHSA	5073 ± 1422	11650 ± 1374
Domain I	1467 ± 205[a]	1804 ± 36[a,b]
Domain II	727 ± 80[a]	5851 ± 1320[a]
Domain III	1110 ± 261[a]	1897 ± 171[a,b]

5 μM rHSA or individual domains was incubated with DHT (20 μM, 0.4 μCi) for 90 minutes and enzymatic activity was measured at 37°C. All values are the mean ± SD (n = 3).
[a] $p < 0.01$ vs. rHSA.
[b] $p < 0.01$ vs. domain II.

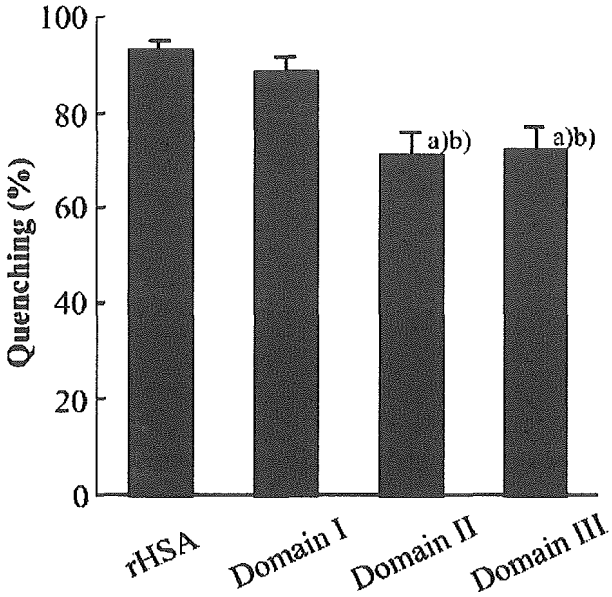

Fig. 3. Quenching of H_2O_2 oxidation of DRD by rHSA and individual domains. The sample solutions contained 7.5 μM rHSA or individual domains in 67 mM sodium phosphate buffer (pH 7.4 and 25°C), 5 μM DRD, and 25 mM H_2O_2. Each bar represents the mean ± SD (n = 3). a) $p < 0.01$ vs. rHSA; b) $p < 0.01$ vs. domain I.

DISCUSSION

The effectiveness of recombinant protein pharmaceuticals is heavily dependent on the intrinsic pharmacokinetics of the natural protein. For example, the efficacy of a drug is affected by its serum half-life. A variety of strategies have been proposed to create long-acting forms of drugs. One approach involves modification of drug formulation so that the product is slowly released from the injection site. This sustained release form requires fewer injections. However, the active agent is not changed, so elimination of the drug remains unchanged and the drug dose must be increased to cover the longer dosing interval. Another strategy is to exploit plasma protein binding; for example, noncovalent association with albumin extends the half-life of short-lived proteins. The drug is covalently linked with a component that is known to bind with high affinity to a plasma protein. Recombinant fusion of the albumin-binding domain of streptococcal protein G (which selectively binds to albumin with high affinity) to human complement receptor type 1 has been shown to increase the half-life of this receptor 3-fold to 5 h in rats (26). In another study, when insulin was acylated with myristic acids, its effects were prolonged due to its spontaneous association with albumin (27). Another approach is to modify the drug itself, so that the active drug is cleared more slowly from the systemic circulation. Because the kidney generally filters out molecules smaller than 60 kDa, efforts to reduce clearance have focused on increasing the molecular size of drugs through protein fusion, glycosylation or addition of polyethylene glycol polymers (*i.e.* PEG). Another approach is conjugation of the drug to a carrier protein to form a prodrug (5,28,29).

Table V. Clearance of ^{111}In-Labeled rHSA and Individual Domains

HSA	Clearance (μl/min)		
	Total	Liver	Kidney
rHSA	3.65 ± 0.78	0.69 ± 0.21	0.28 ± 0.10
Domain I	178.35 ± 9.72[a]	5.12 ± 0.98[b,c]	147.33 ± 10.57[a]
Domain II	181.37 ± 12.12[a]	5.20 ± 2.52[c]	173.38 ± 12.35[a,d]
Domain III	184.80 ± 15.21[a]	19.09 ± 4.16[a]	171.14 ± 5.63[a,d]

All values are mean ± SD (n = 3).
[a] $p < 0.01$ vs. rHSA.
[b] $p < 0.05$ vs. rHSA.
[c] $p < 0.01$ vs. domain III.
[d] $p < 0.05$ vs. domain I.

One of the challenges for the successful commercialization of therapeutic proteins is to maintain the safety and efficacy of the protein during its manufacturing, storage and administration. To achieve this, the purified form of the protein drug is usually formulated with carefully selected excipients. The formulation of a peptide drug preparation would require the inclusion of an antioxidant to maintain the potency of the drug as well as a lyoprotectant. A protein carrier that possesses considerable antioxidant activity could eliminate or reduce use of antioxidants in the formulation. A protein drug carrier with low or no enzymatic activity would promote the stability of a peptide drug or the peptide linker during storage, and may eliminate the need for refrigeration during storage. Low ligand binding capacity of a protein carrier may prevent accumulation of endogenous or exogenous substances which may modify the drug properties during the preparation stage or upon administration into the general circulation. Because proteins have complex molecular structures that can influence the protein stability, the development of stable formulations of protein pharmaceuticals requires an intimate knowledge of the protein structure as well as its chemical and physical properties. In particular, an understanding of the mechanisms by which a protein may degrade is crucial for designing and testing drug formulations. The major pathways of protein degradation include denaturation, aggregation, oxidation and interfacial damage.

Ligand Binding Properties

HSA is the most abundant plasma protein, and is involved in a variety of physiologic functions including maintenance of colloid osmotic pressure. One of its prominent physiologic functions is ligand transport. HSA has at least two distinct binding sites for several physiologically important compounds and a large number of hydrophobic drugs. These two major binding regions, site I and II, are located within specialized cavities in subdomain IIA and IIIA, respectively (1). Although mapping of the locations of each drug binding site had been attempted in qualitative ligand binding studies involving induced circular dichroism using recombinant domains by Dockal *et al.*, quantitative data has not been obtained.

In the current study, all domains showed a significant decrease in the percentage of ligand bound for all site I probes, compared with rHSA, except for the binding of *n*-butyl *p*-AB, a site Ic ligand that binds to domain II. It appears highly likely that the observed marked loss of the ligand binding ability of domain II, which contains site I, is due to the absence of the neighboring domain, which indicates the importance of interdomain interactions for maintaining the

structural stability of site I, particularly at subsites Ia and Ib. The importance of interdomain interactions for the integrity of site I was also indicated by the marked decrease in the intrinsic fluorescence spectra of Trp-214, the only Trp residue of HSA that is located in domain II, reflecting major changes in the environment and dynamics of the residue (Fig. 2). A corresponding decrease in the percentage of warfarin (a site I ligand that has been shown to interact with Trp-214) bound by domain II was also observed.

Domain III, which contains site II, retained most of its ability to bind site II ligands (Table II). The preservation of the binding ability of site II may be due to its structural independence, as indicated by the crystal structure of HSA. The entrance of the binding pocket of site II in domain III is in direct contact with the bulk solvent. In contrast, domain I is in contact with the entrance of the site I binding pocket in domain II (1). However, interactions between domain III and domain II also contribute to the binding of ligands to site II, as indicated by the fact that the bound percentage of site II ligand was lower than that of rHSA.

On the other hand, domain I showed negligible binding to all the ligands used in the binding studies. Kjeldsen *et al.* (30) reported that domain III, but not domain I, binds myristic acid. However, insulin acylated with myristic acid bound to domain III but bound more weakly to domain I.

Enzymatic Activity

Domain III of HSA has been reported to possess esterase-like activity. Arg-410 and Tyr-411 have been identified as the key amino acid residues responsible for the esterase-like activity of domain III. Recently, Watanabe *et al.* (18) reported that the enzymatic activity of albumin is much more dependent on the presence of Tyr-411 than on Arg-410. In the present study, the esterase-like activity of domain III was only about 40% that of the intact rHSA (Table III). This suggests that interdomain interaction is crucial for complete esterase-like activity.

On the other hand, esterase-like activity was also detected in domain I, although it was much weaker than that of domain III. However, the enzymatic site on domain I has not been identified. This esterase-like activity of domain I may be additive to the lower activity found in domain III, as indicated by the much higher total activity observed for intact HSA. However, the formation of a new active site in domain I upon fragmentation cannot be ruled out.

No enzymatic activity was detected for domain II, suggesting the absence of an active site in this domain. This finding is consistent with the fact that domain II has not been reported to possess esterase-like activity in studies of intact HSA.

The enolase-like activity of HSA for DHT has been reported to decrease with polymerization of HSA in malignant breast tumors, compared with benign breast tumors (13). All domains showed a decrease in enolase-like activity at a pH of 7.4 in phosphate buffer, with domain II showing the lowest value, compared with rHSA. In contrast, all domains and rHSA showed an increase in activity at a pH of 9.2 in carbonate buffer. Among the domains, domain II showed the largest increase, suggesting that an enolase active site is generated in domain II upon pH alteration (Table IV).

Antioxidant Properties

HSA is a mixture of mercaptalbumin (which has one free sulfhydryl group at Cys-34) and non-mercaptalbumin (which has a mixed disulfide with cysteine and glutathione at Cys-34 in serum). The fraction of human mercaptalbumin has been shown to be markedly decreased in various diseases including diabetes mellitus, and in some physiologic conditions such as aging, compared with healthy young male subjects (31). In a previous study, we used several different methods to oxidize HSA, and found that Cys-34 and Met residues are major participants in oxidative stress (10).

The antioxidant activity of domain I was found to be slightly lower than that of rHSA. Domain II was found to have antioxidant activity comparable to that of domain III but lower than that of domain I. Each domain contains two Met residues that are thought to contribute to antioxidant activity. The substantial activity of the domains may be due to a more open environment, resulting in a more exposed location of the two methionine residues, allowing them to function as antioxidants more easily. Cys-34 seems to contribute additively to the higher antioxidant activity of domain I, because domain I contains Cys-34 with a free thiol group (Fig. 4).

In the formulation of biotechnological products, albumin has been commonly used as an anti-adhesion agent and lyoprotectant. Other excipients such as nonionic surfactants have also been widely used in the development of protein pharmaceuticals. However, the low level of residual peroxides in surfactants may affect the stability of oxidation-sensitive proteins. In this respect, albumin may also function as an antioxidant, minimizing the potential undesired effects of other excipients.

Pharmacokinetics of Individual Domains

Characterization of the pharmacokinetics and pharmacodynamics of each domain of HSA will facilitate further development of drug targeting strategies. Manipulation of the size of the carrier protein may also be used to control the clearance of the conjugated drug in a graded manner. Sheffield *et al.* (32) tested the effects of truncation on the *in vivo* clearance of rabbit serum albumin (RSA) in rabbits, using recombinant RSA mini-proteins containing the first, first and second, or third domain of the protein. They reported that

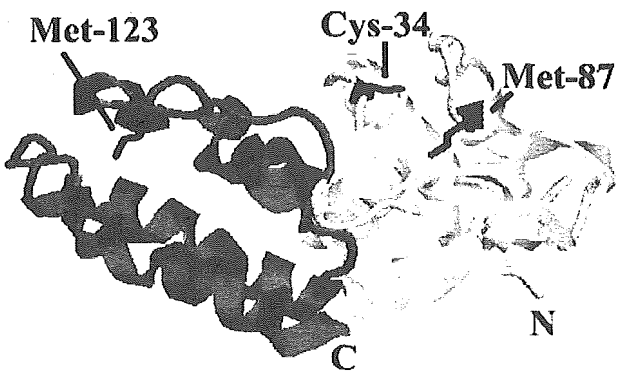

Fig. 4. Ribbon model of domain I. The subdivision of the protein into subdomains (IA and IB) indicated by color codes; N and C represent the N- and C-terminus, respectively. The figure was prepared with Molscript on the basis of the atomic coordinates 1UOR available at the Brookhaven Protein Data Bank.

half-lives did not differ among the truncated proteins, suggesting that all had been reduced below the size threshold.

In the present pharmacokinetic analysis, all three ^{111}In-radiolabeled domains exhibited very rapid elimination compared to rHSA, with a high level of accumulation in the kidney. Domain I showed a slightly lower renal clearance than the other two domains. Domain III showed about a 4-fold higher liver clearance than the other two domains (Table V). Our laboratory has recently shown that the triple-residue mutant K199A/K439A/K525A of rHSA mimics the effect of glycosylation, a reaction that alters the pharmacokinetics of proteins. This suggests that the half-lives of the recombinant domains can be manipulated by mutating certain residues such as positively charged lysine residues (33).

CONCLUSIONS

Domain I of HSA has great potential for further development as a "stand-alone" protein for potential use as a drug delivery protein carrier due to its antioxidative activity and low enzymatic activity. In addition, the presence of a free cysteine residue allows relatively easy conjugation with a drug containing a free thiol moiety. Though its short half-life may make it suitable for application as a stabilizer, polymerization may be a feasible approach for increasing the half-life of domain I protein of HSA.

ACKNOWLEDGMENTS

We wish to thank Dr. Nozomi Koganesawa, Division of Biological Sciences, Hokkaido University, for providing helpful advice about expression and purification. We also wish to thank the members of the Gene Technology Center in Kumamoto University for their important contributions to these experiments.

REFERENCES

1. T. Peters Jr. *All about Albumin: Biochemistry, Genetics, and Medical Applications*, Academic Press, San Diego, 1996.
2. F. Kratz, J. Drevs, G. Bing, C. Stockmar, K. Scheuermann, P. Lazar, and C. Unger. Development and in vitro efficacy of novel MMP2 and MMP9 specific doxorubicin albumin conjugates. *Bioorg. Med. Chem. Lett.* **11**:2001–2006 (2001).
3. P. Kremer, G. Hartung, U. Bauder-Wust, H. H. Schrenk, A. Wunder, S. Heckl, U. Zillmann, and H. Sinn. Efficacy and tolerability of an aminopterin-albumin conjugate in tumor-bearing rats. *Anticancer Drugs* **13**:615–623 (2002).
4. A. Wunder, U. Muller-Ladner, E. H. Stelzer, J. Funk, E. Neumann, G. Stehle, T. Pap, H. Sinn, S. Gay, and C. Fiehn. Albumin-based drug delivery as novel therapeutic approach for rheumatoid arthritis. *J. Immunol.* **170**:4793–4801 (2003).
5. B. L. Osborn, H. S. Olsen, B. Nardelli, J. H. Murray, J. X. Zhou, A. Garcia, G. Moody, L. S. Zaritskaya, and C. Sung. Pharmacokinetic and pharmacodynamic studies of a human serum albumin-interferon-α fusion protein in cynomolgus monkeys. *J. Pharmacol. Exp. Ther.* **303**:540–548 (2002).
6. B. L. Osborn, L. Sekut, M. Corcoran, C. Poortman, B. Sturm, G. Chen, D. Mather, H. L. Lin, and T. J. Parry. Albutropin: a growth hormone-albumin fusion with improved pharmacokinetics and pharmacodynamics in rats and monkeys. *Eur. J. Pharmacol.* **456**: 149–158 (2002).
7. W. Halpern, T. A. Riccobene, H. Agostini, K. Baker, D. Stolow, M. L. Gu, J. Hirsch, A. Mahoney, J. Carrell, E. Boyd, and K. J. Grzegorzewski. Albugranin, a recombinant human granulocyte colony stimulating factor (G-CSF) genetically fused to recombinant human albumin induces prolonged myelopoietic effects in mice and monkeys. *Pharm. Res.* **19**:1720–1729 (2002).
8. P. Yeh, D. Landais, M. Lemaitre, I. Maury, J. Y. Crenne, J. Becquart, A. Murry-Brelier, F. Boucher, G. Montay, R. Fleer, P. H. Hirel, J. F. Mayaux, and D. Klatzmann. Design of yeast-secreted albumin derivatives for human therapy: Biological and antiviral properties of a serum albumin-CD4 genetic conjugate. *Proc. Natl. Acad. Sci. USA* **89**:1904–1908 (1992).
9. E. G. DeMaster, B. J. Quast, B. Redfern, and H. T. Nagasawa. Reaction of nitric oxide with the free sulfhydryl group of human serum albumin yields a sulfenic acid and nitrous oxide. *Biochemistry* **34**:11494–11499 (1995).
10. M. Anraku, K. Yamasaki, T. Maruyama, U. Kragh-Hansen, and M. Otagiri. Effect of oxidative stress on the structure and function of human serum albumin. *Pharm. Res.* **18**:632–639 (2001).
11. K. Ikeda, Y. Kurono, Y. Ozeki, and T. Yotsuyanagi. Effects of drug bindings on esterase activity of human serum albumin. Dissociation constants of the complexes between the protein and drugs such as N-arylanthranilic acids, coumarin derivatives and prostaglandins. *Chem. Pharm. Bull.* **27**:80–87 (1979).
12. Y. Kurono, I. Kushida, H. Tanaka, and K. Ikeda. Esterase-like activity of human serum albumin. VIII. Reaction with amino acid *p*-nitrophenyl esters. *Chem. Pharm. Bull.* **40**:2169–2172 (1992).
13. Z. Drmanovic, S. Voyatzi, D. Kouretas, D. Sahpazidou, A. Papageorgiou, and O. Antonoglou. Albumin possesses intrinsic enolase activity towards dihydrotestosterone which can differentiate benign from malignant breast tumors. *Anticancer Res.* **19**: 4113–4124 (1999).
14. M. Dockal, D. C. Carter, and F. Ruker. The three recombinant domains of human serum albumin. Structural characterization and ligand binding properties. *J. Biol. Chem.* **274**:29303–29310 (1999).
15. M. Dockal, M. Chang, D. C. Carter, and F. Ruker. Five recombinant fragments of human serum albumin - Tools for the characterization of the warfarin binding site. *Protein Sci.* **9**:1455–1465 (2000).
16. S. M. Twine, M. G. Gore, P. Morton, B. C. Fish, A. G. Lee, and J. M. East. Mechanism of binding of warfarin enantiomers to recombinant domains of human albumin. *Arch. Biochem. Biophys.* **414**:83–90 (2003).
17. J. S. Stamler, O. Jaraki, J. Osborne, D. I. Simon, J. Keaney, J. Vita, D. Singel, C. R. Valeri, and J. Loscalzo. Nitric oxide circulates in mammalian plasma primarily as an S-nitroso adduct of serum albumin. *Proc. Natl. Acad. Sci. USA* **89**:7674–7677 (1992).
18. H. Watanabe, S. Tanase, K. Nakajou, T. Maruyama, U. Kragh-Hansen, and M. Otagiri. Role of arg-410 and tyr-411 in human serum albumin for ligand binding and esterase-like activity. *Biochem. J.* **349**:813–819 (2000).
19. R. F. Chen. Removal of fatty acids from serum albumin by charcoal treatment. *J. Biol. Chem.* **242**:173–181 (1967).
20. Y. Takakura, T. Fujita, M. Hashida, and H. Sezaki. Disposition characteristics of macromolecules in tumor-bearing mice. *Pharm. Res.* **7**:339–346 (1990).
21. J. R. Duncan and M. J. Welch. Intracellular metabolism of indium-111-DTPA-labeled receptor targeted proteins. *J. Nucl. Med.* **34**:1728–1738 (1993).
22. K. Yamaoka, Y. Tanigawara, T. Nakagawa, and T. Uno. A pharmacokinetic analysis program (multi) for microcomputer. *J. Pharmacobiodyn.* **4**:879–885 (1981).
23. T. Mukai, Y. Arano, K. Nishida, H. Sasaki, H. Saji, and J. Nakamura. In-vivo evaluation of indium-111-diethylene-triaminepentaacetic acid-labelling for determining the sites and rates of protein catabolism in mice. *J. Pharm. Pharmacol.* **51**:15–20 (1999).
24. K. Yamasaki, T. Maruyama, U. Kragh-Hansen, and M. Otagiri. Characterization of site I on human serum albumin: concept about the structure of a drug binding site. *Biochim. Biophys. Acta* **1295**:147–157 (1996).
25. R. J. Hondal, A. K. Motley, K. E. Hill, and R. F. Burk. Failure of selenomethionine residues in albumin and immunoglobulin G to protect against peroxynitrite. *Arch. Biochem. Biophys.* **371**:29–34 (1999).

26. S. C. Makrides, P. A. Nygren, B. Andrews, P. J. Ford, K. S. Evans, E. G. Hayman, H. Adari, H. Adari, M. Uhlen, and C. A. Toth. Extended *in vivo* half-life of human soluble complement receptor type 1 fused to a serum albumin-binding receptor. *J. Pharmacol. Exp. Ther.* **277**:534–542 (1996).
27. P. Kurtzhals, S. Havelund, I. Jonassen, B. Kiehr, U. D. Larsen, U. Ribel, and J. Markussen. Albumin binding of insulins acylated with fatty acids: characterization of the ligand-protein interaction and correlation between binding affinity and timing of the insulin effect *in vivo*. *Biochem. J.* **312**:725–731 (1995).
28. L. Beljaars, G. Molema, B. Weert, H. Bonnema, P. Olinga, G. M. Groothuis, D. K. Meijer, and K. Poelstra. Albumin modified with mannose 6-phosphate: A potential carrier for selective delivery of antifibrotic drugs to rat and human hepatic stellate cells. *Hepatology* **29**:1486–1493 (1999).
29. H. Sakai, S. Takeoka, S. I. Park, T. Kose, H. Nishide, Y. Izumi, A. Yoshizu, K. Kobayashi, and E. Tsuchida. Surface modification of hemoglobin vesicles with poly(ethylene glycol) and effects on aggregation, viscosity, and blood flow during 90% exchange transfusion in anesthetized rats. *Bioconjug. Chem.* **8**:23–30 (1997).
30. T. Kjeldsen, A. F. Pettersson, L. Drube, P. Kurtzhals, I. Jonassen, S. Havelund, P. H. Hansen, and J. Markussen. Secretory expression of human albumin domains in *Saccharomyces cerevisiae* and their binding of myristic acid and an acylated insulin analogue. *Protein Expr. Purif.* **13**:163–169 (1998).
31. E. Suzuki, K. Yasuda, N. Takeda, S. Sakata, S. Era, K. Kuwata, M. Sogami, and K. Miura. Increased oxidized form of human serum albumin in patients with diabetes mellitus. *Diabetes Res. Clin. Pract.* **18**:153–158 (1992).
32. W. P. Sheffield, J. A. Marques, V. Bhakta, and I. J. Smith. Modulation of clearance of recombinant serum albumin by either glycosylation or truncation. *Thromb. Res.* **99**:613–621 (2000).
33. K. Nakajou, H. Watanabe, U. Kragh-Hansen, T. Maruyama, and M. Otagiri. The effect of glycation on the structure, function and biological fate of human serum albumin as revealed by recombinant mutants. *Biochim. Biophys. Acta* **1623**:88–97 (2003).

THE JOURNAL OF BIOLOGICAL CHEMISTRY
Vol. 280, No. 2, Issue of January 14, pp. 1384–1391, 2005
Printed in U.S.A.

Use of Photoaffinity Labeling and Site-directed Mutagenesis for Identification of the Key Residue Responsible for Extraordinarily High Affinity Binding of UCN-01 in Human α1-Acid Glycoprotein*

Received for publication, September 27, 2004, and in revised form, October 26, 2004
Published, JBC Papers in Press, October 27, 2004, DOI 10.1074/jbc.M411076200

Masaaki Katsuki‡, Victor Tuan Giam Chuang‡§, Koji Nishi‡, Kohichi Kawahara¶, Hitoshi Nakayama¶, Noriyuki Yamaotsu‖, Shuichi Hirono‖, and Masaki Otagiri‡**

From the Departments of ‡Biopharmaceutics and ¶Molecular Cell Function, Graduate School of Medical and Pharmaceutical Sciences, Kumamoto University, 5-1 Oe-honmachi, Kumamoto, 862-0973, Japan, the §Department of Pharmacy, Faculty of Allied Health Sciences, Universiti Kebangsaan Malaysia, Jalan Raja Muda Abdul Aziz, 50300 Kuala Lumpur, Malaysia, and ‖The School of Pharmaceutical Sciences, Kitasato University, 5-9-1, Shirokane, Minato-ku, Tokyo, 108-8641, Japan

7-Hydroxystaurosporine (UCN-01) is a protein kinase inhibitor anticancer drug currently undergoing a phase II clinical trial. The low distribution volumes and systemic clearance of UCN-01 in human patients have been found to be caused in part by its extraordinarily high affinity binding to human α1-acid glycoprotein (hAGP). In the present study, we photolabeled hAGP with [^{3}H]UCN-01 without further chemical modification. The photolabeling specificity of [^{3}H]UCN-01 was confirmed by findings in which other hAGP binding ligands inhibited formation of covalent bonds between hAGP and [^{3}H]UCN-01. The amino acid sequence of the photolabeled peptide was concluded to be SDVVYTDXK, corresponding to residues Ser-153 to Lys-161 of hAGP. No PTH derivatives were detected at the 8th cycle, which corresponded to the 160th Trp residue. This strongly implies that Trp-160 was photolabeled by [^{3}H]UCN-01. Three recombinant hAGP mutants (W25A, W122A, and W160A) and wild-type recombinant hAGP were photolabeled by [^{3}H]UCN-01. Only mutant W160A showed a marked decrease in the extent of photoincorporation. These results strongly suggest that Trp-160 plays a prominent role in the high affinity binding of [^{3}H]UCN-01 to hAGP. A docking model of UCN-01 and hAGP around Trp-160 provided further details of the binding site topology.

Human α1-acid glycoprotein (hAGP)[1] is an acute phase protein with a molecular mass of 41 to 43 kDa and is heavily glycosylated (45%) (1). It contains sialic acids, which cause it to be negatively charged (pI = 2.7~3.2) (2). Its glycosylation pattern can change depending on the type of inflammation (3). The biological function of hAGP is not clear, although studies using *in vivo* models of inflammation indicate that it plays anti-inflammatory and immunomodulating roles and has protective effects (4, 5). The "basal" level of hAGP is ~20 μmol/liter, but hAGP levels can increase by 5–10-fold in response to stress, infection, or an inflammatory response to neoplasm (6, 7). In addition to increases in hAGP plasma concentration in certain cancers, changes in the expression of genetic variants of hAGP can occur according to the specific type of cancer (8). The levels of hAGP vary widely and heterogeneously among cancer patients; according to the type of disease, the composition of hAGP consists of various isoforms and degrees of glycosylation (9). Studies have shown that increases in circulating hAGP alter the pharmacokinetic disposition and pharmacological action of numerous drugs that bind to it (10–12). For example, increased hAGP levels associated with advanced tumors alter the pharmacokinetics of Imatinib (STI571), a tyrosine kinase inhibitor, in leukemia patients (13). hAGP also appears to be an independent predictor of response and a major objective prognostic factor of survival in patients with non-small cell lung cancer treated with docetaxel chemotherapy (14). Thus, hAGP is an important modulator of drug pharmacokinetics and pharmacodynamics in anticancer therapeutics.

7-Hydroxystaurosporine (UCN-01) has an indolocarbazole moiety and was originally isolated as a selective inhibitor of a Ca^{2+}- and phospholipid-dependent protein kinase (protein kinase C (PKC)) (15). UCN-01 is a derivative of staurosporine, which occurs naturally, inhibits numerous other kinases, and has greater selectivity for PKC than does staurosporine (16, 17). UCN-01 can mediate 3 distinct cellular effects *in vitro*: cell cycle arrest, induction of apoptosis, and potentiation of DNA damage-related toxicity (18–20). It exhibits anticancer activity against human and murine tumor cell lines that have aberrations in cellular signal transduction (21–24). Unlike other compounds with an indolocarbazole moiety, UCN-01 preferentially induces G_1 phase accumulation in various cell lines, and one of its mechanisms of action is clearly mediated by dephosphorylation of retinoblastoma protein and inhibition of cyclin-dependent kinase 2 (CDK2), an intracellular retinoblastoma protein kinase that regulates the transition from the G_1 to S phase (25). In addition, UCN-01 enhances the anticancer effects of several important chemotherapeutic drugs, including mitomycin C, cisplatin, and 5-fluorouracil, *in vitro* and *in vivo* (26–28). UCN-01 is currently in the phase II study of its effects on relapsed or refractory systemic anaplastic large cell and mature T-cell lymphomas (29, 30). UCN-01 was initially administered as a 72-h continuous infusion every 2 weeks, based on data from *in vitro* and xenograft preclinical models. However, in the first few patients, the drug had an unexpectedly long half-life (>30 days), which was 100 times longer than the

* The costs of publication of this article were defrayed in part by the payment of page charges. This article must therefore be hereby marked "*advertisement*" in accordance with 18 U.S.C. Section 1734 solely to indicate this fact.

** To whom correspondence should be addressed: Dept. of Biopharmaceutics, Graduate School of Pharmaceutical Sciences, Kumamoto University, 5-1 Oe-honmachi, Kumamoto, 862-0973, Japan. Tel.: 81-96-3714150; Fax: 81-96-3627690; E-mail: otagirim@gpo.kumamoto-u.ac.jp.

[1] The abbreviations used are: hAGP, human α1-acid glycoprotein; UCN-01, 7-hydroxystaurosporine; rhAGP, recombinant hAGP; PVDF, polyvinylidene difluoride; HPLC, high performance liquid chromatography; PKC, protein kinase C.

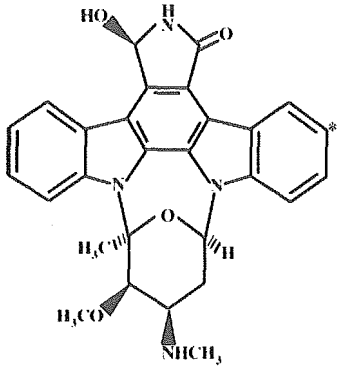

FIG. 1. **Chemical structure of [^{3}H]UCN-01.** *, ^{3}H-labeled position.

half-life observed in preclinical models. The distribution volumes (0.0796~0.158 liter/kg) and systemic clearance (0.0407~0.252 ml/h/kg) in the human patients were found to be extremely low. This pharmacokinetic behavior of UCN-01 in humans can partly be attributed to its specific high affinity binding to hAGP, which causes slow dissociation of UCN-01 from hAGP and thereby limits its disposition and elimination (31, 32). The binding constant for UCN-01 and hAGP, 8×10^8 M^{-1}, is the highest value ever reported for protein binding studies (33).

Several protein binding studies of hAGP had been conducted using a variety of techniques including equilibrium dialysis, ultrafiltration, chemical modification, and displacement (34–37). In a recent study, we identified the key factors contributing to the unusually high binding affinity between UCN-01 and hAGP: the substituent at C-7 of the UCN-01 molecule, and the Trp residues of hAGP (38). Crystallographic structural analysis has become more common and appears to be a good method for analysis of ligand-protein interaction, but there have been no reports of crystallographic structural analysis of hAGP. Certain experimental techniques allow direct evaluation of ligand-protein complexes, which can elucidate the binding chemistry of hAGP. Photoaffinity labeling is an essential complement to modeling and mutagenesis and allows direct, unambiguous identification of the contact region between a binding protein and its specific photoactivatable ligands (39–41). There is no photoaffinity labeling study that has led to the direct determination of labeled amino acid residues in hAGP. In the present study, we used [^{3}H]UCN-01 (Fig. 1) as a photoaffinity labeling agent to characterize the binding site of hAGP. Also, single residue mutants of recombinant hAGP (W25A, W122A, and W160A) were produced in order to determine which Trp was involved in the high affinity binding of [^{3}H]UCN-01. Finally, we constructed models of the docking of UCN-01 into the binding cavity, using a three-dimensional molecular model of hAGP.

EXPERIMENTAL PROCEDURES

Materials—[^{3}H]UCN-01 (12 Ci/mmol), UCN-01, UCN-02, and staurosporine were supplied by Kyowa Hakko Kogyo Co. (Shizuoka, Japan). hAGP (purified from cohn fraction VI) was purchased from Sigma. Sequencing grade modified trypsin was purchased from Promega. All other chemicals and solvents were of analytical grade. *N*-Glycosidase F recombinant (PNGase F) was purchased from Roche Applied Science. Plasma-derived AGP (pAGP), propranolol, and progesterone were purchased from Sigma. Potassium warfarin was donated by Eisai Co. (Tokyo, Japan). Restriction enzymes, *Escherichia coli* JM109, the DNA ligation kit, and the DNA polymerase Premix Taq® (EX Taq version) were obtained from Takara Biotechnology Co. Ltd. (Kyoto, Japan). The DNA sequencing kit was obtained from PerkinElmer Applied Biosystems (Tokyo, Japan). The Pichia expression kit was purchased from Invitrogen. DEAE Sephacel, phenyl-Sepharose Fast Flow, and Sephadex G-75 superfine were purchased from Amersham Biosciences.

Expression and Purification of Wild-type and Mutant rhAGP—Recombinant hAGP (rhAGP) was expressed in the methylotropic yeast *Pichia pastoris* using the expression vector pPIC9, and was purified by anionic exchange, hydrophobic interaction, and gel filtration chromatography (42). The single residue mutants W25A, W122A, and W160A were prepared using a QuikChange® XL site-directed mutagenesis kit, following the procedure of Braman *et al.* (43).

Purification of rhAGP—The growth medium was separated from the yeast by centrifugation (6000 × *g*, 10 min, 4 °C), and the secreted rhAGP was isolated from the medium as follows. The medium was brought to 60% saturation with ammonium sulfate at room temperature. The temperature was then lowered to 4 °C, and the pH was adjusted to 4.0. After shaking for 12 h, the precipitated protein was collected by centrifugation (12,000 × *g*, 60 min, 4 °C) and resuspended in distilled water. Dialysis was performed for 48 h at 4 °C against 100 volumes of distilled water, followed by a further 24 h of dialysis against 100 volumes of 10 mM Tris-HCl buffer (pH 7.4). Then, the solution was loaded onto a column of DEAE Sephacel. rhAGP was eluted with a linear gradient of 0–1 M NaCl in 10 mM Tris-HCl buffer (pH 7.4). The eluted rhAGP was loaded onto a column of phenyl-Sepharose Fast Flow. Finally, rhAGP was purified using Sephadex G-75 superfine resin.

Photoaffinity Labeling of hAGP—hAGP (50 μM) was incubated with [^{3}H]UCN-01 (0.08 μM) in 100 μl of 20 mM Tris-HCl (pH 7.4) in a 1.5-ml Eppendorf tube at room temperature in the dark for 60 min. The incubation mixture was then placed on ice and irradiated for 30 min by a 100-watt black light/blue lamp (310 nm, Ultra-Violet Products, Inc., San Gabriel, CA) at a distance of 10 cm. After irradiation, the photolabeled hAGP was precipitated by adding 1 ml of acetone, followed by centrifugation at 15 × 1000 rpm for 10 min. The pellet was washed with 1 ml of ethanol and centrifuged a second time.

SDS-PAGE and Electroblotting—Photolabeled hAGP was analyzed by SDS-PAGE using a 10% polyacrylamide gel (according to the method of Laemmli) and a sampling buffer (10 mM Tris-HCl, pH 7.6, 1% (w/v) SDS, 20 mM dithiothreitol, 4 mM EDTA, and 2% (w/v) sucrose). The concentration of protein was determined by Bradford assay using bovine serum albumin as the standard (44). After electrophoresis, the gel was electrophoretically transferred onto a PVDF membrane in a transfer buffer (25 mM Tris, 193 mM glycine, 10% methanol) using a semidry blotting assembly. The blotted membrane was stained with Coomassie Brilliant Blue R250, followed by complete drying in air.

Autoradiograpic Analysis—For autoradiographic analysis, the dried PVDF membrane was placed in contact with an imaging plate (BAS III, Fuji Photo Film Co.) in a cassette (BAS cassette 2040) at room temperature for 48 h. The imaging plate was scanned and analyzed using a Bio-Imaging Analyzer (model BAS FLA-3000 G; Fuji Photo Film Co.), and was then analyzed using L Process V1.6 software (Fuji Film Science Lab 98). The incorporation of radioactivity into individual fragments was quantified using Image Gauge V3.1 software (Fuji Film).

Competition Experiments—In order to determine the photolabeling specificity of the binding site of [^{3}H]UCN-01, hAGP (50 μM) was incubated with [^{3}H]UCN-01 (0.08 μM) in the presence of competitors (250 μM) prior to photolysis. The competitors were the UCN-01 analogues staurosporine and UCN-02, the basic drug propranolol, the acidic drug warfarin, and progesterone (representative steroid hormone). The photolabeled hAGP was separated by 10% gel SDS-PAGE and electroblotted onto a PVDF membrane before being subjected to autoradiographic analysis.

Reductive Pyridylethylation and Deglycosylation of hAGP—After the photolabeled hAGP was precipitated by acetone, 100 μl of the buffer was added to the precipitate. Then, 10 μl of 1% SDS and 1 M 2-mercaptoethanol were added to this solution, followed by reduction at 100 °C at 10 min. For deglycosylation of hAGP, 10 μl of 10% *n*-octanoyl-*N*-methylglucamide (MEGA-8), 50 μl of deionized water and 2 units of PNGase F were added to the reduction solution, and the resulting solution was incubated for 24 h. Then, 1 μl of 4-vinylpyridine was added, the mixture was further incubated in a N_2 atmosphere for 30 min at room temperature in the dark, and was then dialyzed for desalination.

Tryptic Digestion and Purification of Photolabeled hAGP Peptide Fragments—Tryptic digestion was performed in 50 mM NH_4HCO_3 (pH 7.8). After deglycosylation, deglycosylated hAGP was incubated with trypsin for 5 h at 37 °C. The ratio of trypsin to hAGP was 1:20 (w/w). Tryptic peptides were separated by reverse-phase C_{18} column (5 μm, 4.6 × 250 mm, Vydac) high performance liquid chromatography (HPLC) using an aqueous acetonitrile gradient in the presence of 0.1% trifluoroacetic acid. The separated peptides were fractionated every 30 s; 200 μl of each fraction were added to 2.5 ml of scintillation mixture; and the radioactivity was determined using a LSC-500 liquid scintillation counter (Aloka, Tokyo, Japan). The fraction with the highest radioactivity was collected in an Eppendorf tube, and was evaporated on a SpeedVac

evaporator until the volume of the sample was about 50 μl.

Capillary HPLC Separation and Sequencing—After evaporation, 10 μl of the sample was injected into an ABI 173 A MicroBlotter Capillary HPLC System (PerkinElmer Life Sciences) (45). The sample was manipulated according to the manufacturer's instructions (User's Manual, PerkinElmer Life Sciences). Meanwhile, the blotted membrane from the capillary HPLC separation using a C_{18} column (5 μm, 1.5 × 150 mm, PerkinElmer) was in contact with an imaging plate for 48 h prior to autoradiography analysis. The PVDF membrane was aligned with the chromatogram of a peptide map from the ABI 173 A MicroBlotter Capillary HPLC System. Portions of the PVDF membrane were excised for sequencing on an Applied Biosystems Procise Sequencer with reference to the autoradiogram.

Docking of UCN-01 to hAGP—The structure of hAGP has not previously been experimentally determined. As a model of the three-dimensional structure of hAGP for ligand docking, we used the modeled structure of hAGP obtained by Kopecky *et al.* (46). The initial structure of UCN-01 was taken from the crystal structure of the Chk1·UCN-01 complex (47, PDB ID 1NVQ). The docking calculation of UCN-01 to hAGP was performed using the SYBYL FlexX (48) under the condition that UCN-01 interacts with Trp-160. During the docking calculation, the structure of hAGP and the ring conformation of UCN-01 were kept rigid. The docking algorithm produced 158 different placements of UCN-01 in hAGP. All placements were evaluated by SYBYL CScore and were then ranked using AASS (Average of Auto-Scaled Scores), as follows in Equation 1.

$$\mathrm{AASS}^{\mathrm{placement}} = \left| \sum_{i} \frac{i\_Score^{\mathrm{placement}} - \min(i\_Score)}{\max(i\_Score) - \min(i\_Score)} \right| \Big/ n \qquad \text{(Eq. 1)}$$

In the AASS calculation, n = 5 and i = F_Score (48), G_Score (49), PMF_Score (50), D_Score (51), ChemScore (52). Although the top 5 placements had nearly the same AASS values, they were classified into two types of binding modes. For each type, we chose the placement with the best AASS value as the candidate binding mode. In the type I model, UCN-01 is bound to a hydrophobic pocket formed by Val-41, Ile-44, Phe-48, and Val-156. In the type II model, UCN-01 is packed into a hydrophobic pocket consisting of Ile-28, Pro-131, Leu-138, Tyr-157, and Trp-160.

Refinement of Docking Models—To refine the docking models, the coordinates of the atoms of UCN-01 and the atoms of hAGP within 10 Å from UCN-01 were optimized to reduce the root mean square of the gradients of potential energy below 0.05 kcal mol^{-1} Å-1 using SYBYL 6.9.1 (Tripos, Inc., 2003). The Tripos force field was used for the molecular energy calculation. The AMBER 7 charges (53) were used as the atomic charges for hAGP. The Gasteiger-Hückel charges (54–57) were used as the charges for UCN-01. The cut-off distance for the non-bonded interactions was 10 Å. The distance-dependent dielectric constant of 4r was used. Due to the lack of hydrogen atoms in the modeled structure of hAGP, the initial positions of the hydrogen atoms in the hAGP were generated by the SYBYL.

Statistical Analysis—Statistical analysis of differences was performed by one-way ANOVA followed by the modified Fisher's least squares difference method.

RESULTS

Photolabeling of [^{3}H]UCN-01 to hAGP—The autoradiogram in Fig. 2 shows that the band of radiolabeled protein appeared only upon the photoirradiation of hAGP with [^{3}H]UCN-01. The radioactivity band indicated the incorporation of [^{3}H]UCN-01 to hAGP via photoirradiation. No band of radiolabeled protein could be observed for the sample without irradiation indicating that no covalent attachment of [^{3}H]UCN-01 to hAGP occurred in the dark. Exposure to light for 30 min was sufficient for the photoincorporation of [^{3}H]UCN-01 to hAGP (Fig. 3). The results indicate that [^{3}H]UCN-01 is photoactivatable and stable in the dark.

Competition Experiments—In a previous study using ultracentrifugation methods, it was concluded that the binding site for UCN-01 on hAGP partly overlaps with the binding site for basic drugs, acidic drugs, and steroid hormones (58). In the present photolabeling experiment, in order to determine the photolabeling specificity of [^{3}H]UCN-01, we used staurosporine and UCN-02 (a stereoisomer of UCN-01), which also bind

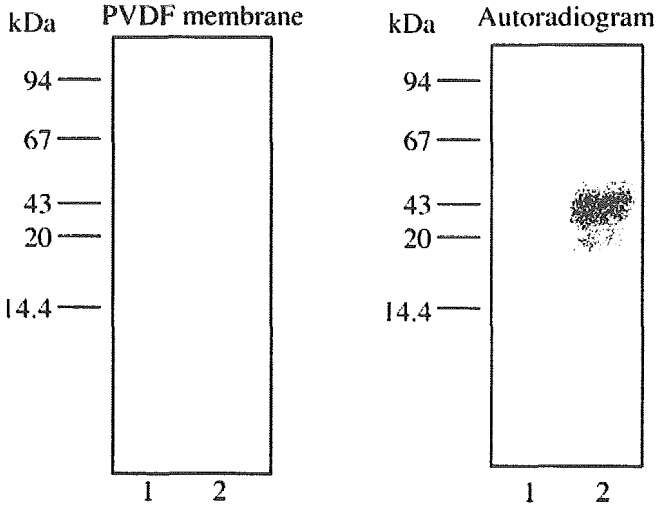

FIG. 2. **Photolabeling of hAGP with [^{3}H]UCN-01.** *Lane 1*, sample taken just prior to photoirradiation. *Lane 2*, sample taken after 30-min photoirradiation (>300 nm). 50 μM hAGP was incubated with 0.08 μM [^{3}H]UCN-01 for 60 min prior to photoirradiation. The samples were separated with 10% SDS-PAGE and electroblotted onto a PVDF membrane for autoradiographic analysis.

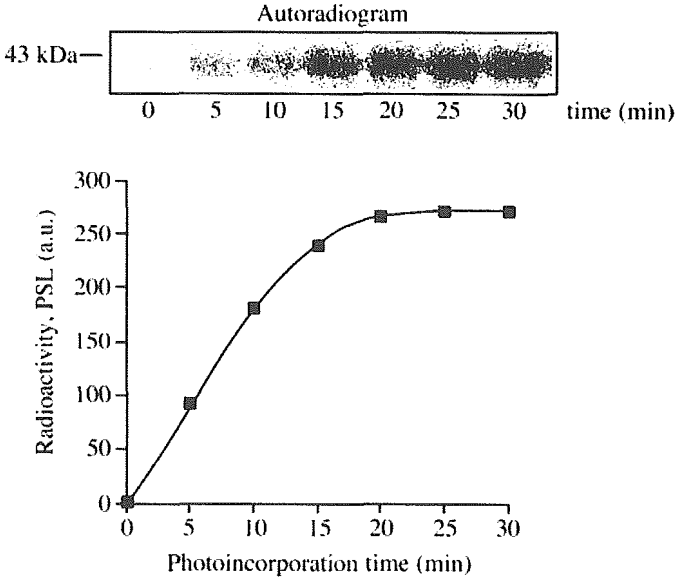

FIG. 3. **Time course of [^{3}H]UCN-01 photoincorporation.** 50 μM hAGP was incubated with 0.08 μM [^{3}H]UCN-01 for 60 min prior to photoirradiation. Aliquots of 100 μl were taken from the mixture solution at each time point as stated in the figure during irradiation until 30 min. All samples were separated with 10% SDS-PAGE and electroblotted onto a PVDF membrane for autoradiographic analysis. *PSL*, photostimulated luminescence.

hAGP, as competitors. All staurosporine analogs significantly inhibited photoincorporation, by more than 60% (Fig. 4). Other competitors that we used were representatives of other hAGP ligands: an acidic drug (warfarin), a basic drug (propranolol), and a steroid (progesterone). Warfarin and propranolol inhibited binding by less than 30%, but to a significant degree, whereas progesterone inhibited binding by about 60% (Table I).

Amino Acid Sequence of the Photolabeled Tryptic Peptides—Tryptic peptides of the hAGP photolabeled with [^{3}H]UCN-01 were separated by reverse phase HPLC using a C_{18} column. The major radioactive peptides were eluted in 10.5–11.5 min (Fig. 5, *A* and *B*). The fractions eluted within this time frame were collected and concentrated with a SpeedVac evaporator for further capillary HPLC analysis. The concentrated sample from previous HPLC analysis was separated and simulta-

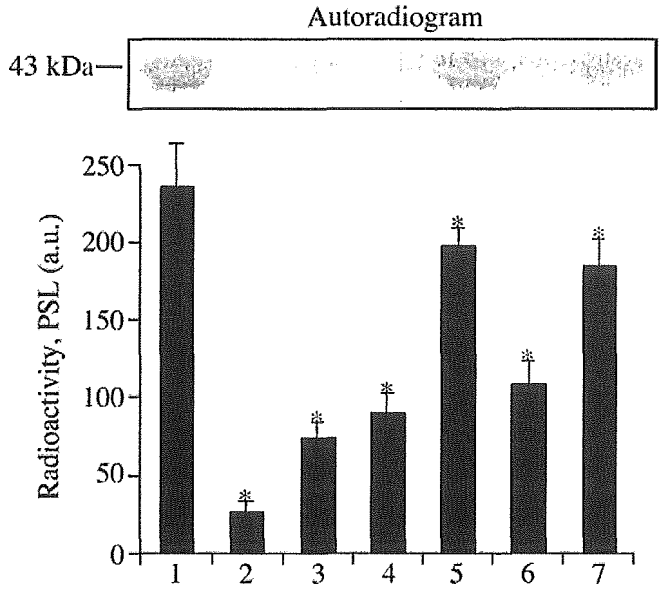

FIG. 4. **Photolabeling of hAGP with [^{3}H]UCN-01 in the presence of competitors.** *Lane 1*, no competitor; *lane 2*, cold UCN-01; *lane 3*, staurosporine; *lane 4*, UCN-02; *lane 5*, warfarin; *lane 6*, progesterone; *lane 7*, propranolol. 50 μM hAGP was incubated with 0.08 μM [^{3}H]UCN-01 and 250 μM competitors for 60 min prior to photoirradiation. The incubation mixture was irradiated for 30 min, separated with 10% SDS-PAGE, and electroblotted onto a PVDF membrane for autoradiographic analysis. *, statistically significant, compared with no competitor; $p < 0.01$. *PSL*, photostimulated luminescence.

TABLE I
Binding affinity constant and inhibition percentage by the competitors

Competitor	K_a	Inhibition
	M^{-1}	%
Cold UCN-01[a]	2.88×10^8	86.38
Staurosporine[a]	1.13×10^7	68.54
UCN-02[a]	1.48×10^6	61.52
Warfarin[b]	1.08×10^6	16.43
Progesterone[b]	1.00×10^5	58.71
Propranolol[b]	2.98×10^5	26.26

[a] Binding constant data taken from Ref. 38.
[b] Binding constant data taken from Ref 59.

neously blotted onto a strip of PVDF membrane using an ABI 173 A MicroBlotter Capillary HPLC System. Autoradiographic analysis of the PVDF membrane indicated that the radioactive spot corresponded to the peak observed at 84–85 min (Fig. 6, *A* and *B*). Edman sequencing of this spot revealed an amino acid sequence of SDVVYTDXK (Fig. 7), corresponding to Ser-153 to Lys-161 of hAGP.

Photolabeling of Wild-type and Mutant rhAGP with [^{3}H]UCN-01—Mutation of the 160th Trp residue of rhAGP to an Ala residue (W160A) caused a significant decrease in photoincorporation, by about 80%. In contrast, there was no significant difference in photoincorporation of [^{3}H]UCN-01 between wild-type rhAGP and the rhAGP mutants W25A and W122A (Fig. 8).

Docking of UCN-01 to hAGP—We constructed models of the docking of UCN-01 into the binding cavity of hAGP around Trp-160, using the three-dimensional molecular model of hAGP published by Kopecky *et al.* (46), to map the possible binding sites of hAGP. Molecular modeling calculations revealed 2 potential binding sites, type I and type II, around Trp-160, both of which were located in the outer region of hAGP (Fig. 9*A*). Table II shows the distance and nature of interaction between donors and acceptors in the models of types I and II. In the type II model, UCN-01 is packed into a surface cleft consisting of Ile-28, Pro-131, Glu-132, Lys-135, Leu-138, Tyr-157, Trp-160,

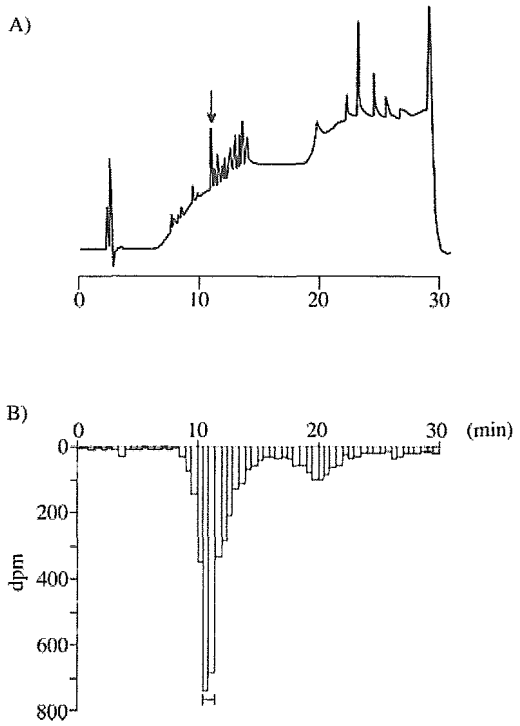

FIG. 5. **Reverse-phase HPLC separation of tryptic peptides of hAGP photolabeled with [^{3}H]UCN-01.** *A*, chromatogram of tryptic peptides of hAGP photolabeled with [^{3}H]UCN-01 detected at UV absorption wavelength of 210 nm. *B*, radioactivity of the reverse-phase fractions (200 μl) was determined by scintillation counting. An aliquot of 20 μl of the tryptic peptides was applied to a C_{18}-column and eluted at 1 ml/min using an aqueous acetonitrile gradient in the presence of 0.1% trifluoroacetic acid (from 5 to 95% acetonitrile over the course of 40 min).

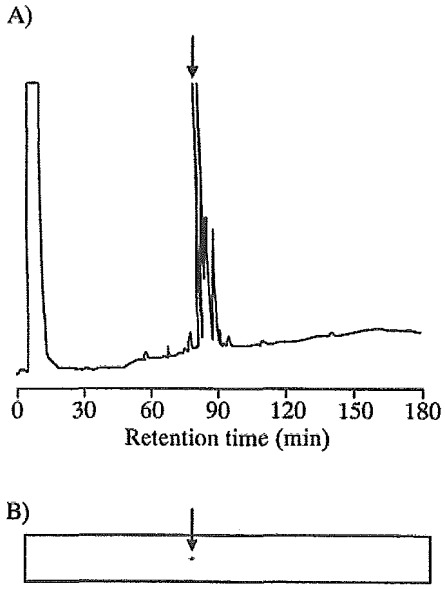

FIG. 6. **Chromatogram of capillary HPLC and autoradiogram of blotted PVDF membrane.** *A*, UV-absorption (210 nm). *B*, autoradiogram of blotted PVDF membrane. After purification of peptides using reverse-phase HPLC, an aliquot of 10 μl of the evaporating sample was applied to a C_{18} column and eluted at 5 μl/min using an aqueous acetonitrile gradient in the presence of 0.1% trifluoroacetic acid (from 5 to 95% acetonitrile over the course of 200 min). The blotted membrane from the capillary HPLC separation was in contact with an imaging plate for 48 h prior to autoradiography analysis.

and Lys-161 (Fig. 9*B*). The surrounding amino acid residues within 5 Å of the UCN-01 molecule include Lys-135, Tyr-157, Trp-160, and Lys-161. The oxygen atom in the sugar ring of

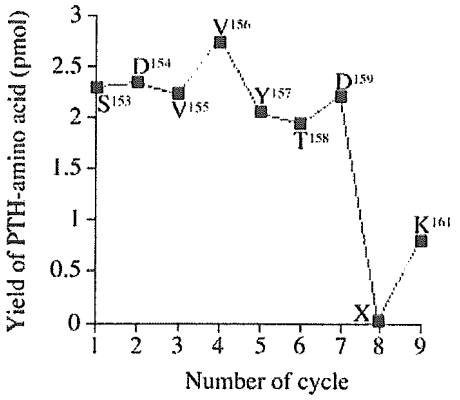

^{150}IPKSDVVYTDWKKDKC^{165}

FIG. 7. **N-terminal amino acid sequence analysis by the Edman degradation method and amino acid sequence of the photolabeled region of hAGP (tryptic peptides).** *PTH*, phenylthiohydantoin.

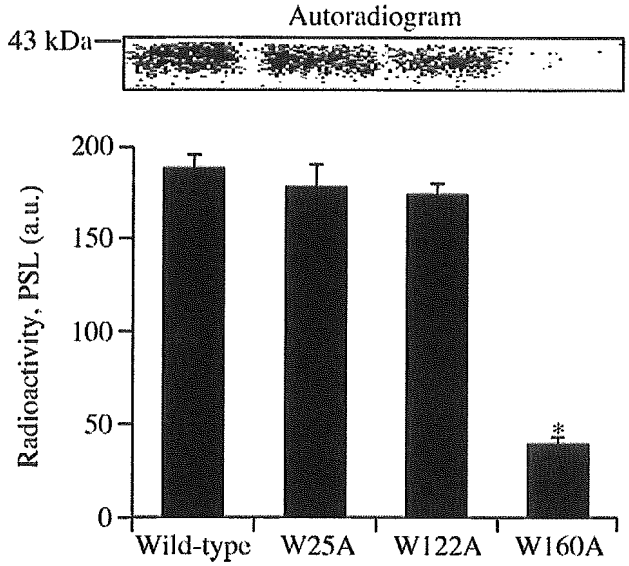

FIG. 8. **Photolabeling of wild type, W25A, W122A, and W160A with [^{3}H]UCN-01.** A sample of 50 μM rhAGP was incubated with 0.08 μM [^{3}H]UCN-01 for 60 min prior to photoirradiation. The samples were separated with 10% SDS-PAGE and electroblotted onto a PVDF membrane for autoradiographic analysis. *, statistically significant, compared with wild type; $p < 0.01$. *PSL*, photostimulated luminescence.

UCN-01 is in contact with Lys-135. The C=O group of UCN-01 was observed to form a hydrogen bond with the amino group of Trp-160, and electrostatic interaction was observed between the amino group of Lys-161 and both the 7-OH group and C=O group of UCN-01. Furthermore, the aromatic ring of UCN-01 is adjacent to Tyr-157 and Trp-160. In contrast, these interactions were not observed in the type I model, in which UCN-01 was shown to be packed into a surface cleft consisting of Val-41, Glu-43, Ile-44, Phe-48, Tyr-50, Val-156, Thr-158, and Trp-160 (data not shown).

DISCUSSION

The acute phase response alters the composition of carrier proteins in plasma, which may affect the blood deposition and transport of biomediators and drugs. Understanding the interaction of drugs with plasma proteins is essential to understanding their systemic pharmacology and toxicology. Thus, information about the effects of the acute phase response on the ligand binding ability of plasma can be used to optimize drug

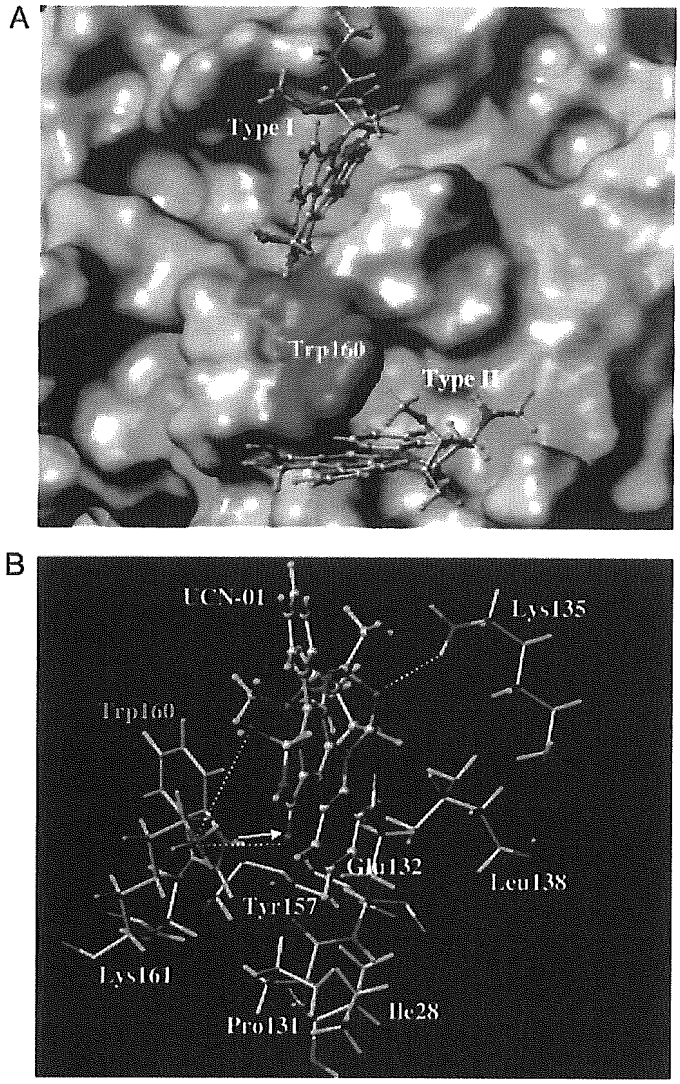

FIG. 9. *A*, type I and II docking models of UCN-01 and hAGP. Hydrophobic amino acids are shown in *green*. *B*, amino acid residues in a surface cleft around Trp-160 that interacts with UCN-01 exhibited in type II docking model. *Dotted line*, electrostatic interaction. *Arrow*, hydrogen bonding.

administration protocols in clinical practice. hAGP has been reported to be a major plasma protein that predominantly binds basic drugs (60). However, protein binding studies suggest that hAGP has 1 wide and flexible drug binding area that accommodates not only basic but also acidic and steroidal drugs (61). A current model of the hAGP binding site depicts a buried pocket with a negatively charged region that interacts with the N termini of basic drugs (62). The tertiary structure of hAGP has proven refractory to resolution, and structure-activity studies using various approaches are needed to clarify the nature of the binding site on this important protein.

The initial treatment protocol for UCN-01 was a 72-h infusion administered at 2-week intervals, because certain cell types (*e.g.* MDA-MB-468 breast carcinoma cells) required 72 h of drug exposure before irreversible growth inhibition occurred (23). However, the clinical outcome of the first 9 patients treated using this schedule demonstrated unexpectedly high concentrations of the drug with a long terminal elimination half-life ($t_{1/2}$). This led to a modification of the UCN-01 administration schedule, in which the recommended phase II dose of UCN-01 is administered as a 72-h continuous infusion at 42.5 mg/m^2/d over a 3-day period. Second and subsequent courses were administered for only 36 h at the same concentration and

TABLE II
Interaction and distance between donors and acceptors in the model of types I and II

Donor	Acceptor	Interaction	Distance
			Å
Type I			
UCN-01@NH_2^+	Glu-43@OE2	Hydrogen bonding	2.793
Tyr-50@OH	UCN-01@C=O	Hydrogen bonding	2.770
Type II			
Trp-160@NE1	UCN-01@C=O	Hydrogen bonding	2.878
Lys-135@NZ	UCN-01@-O-	Electrostatic	4.760
Lys-161@NZ	UCN-01@OH	Electrostatic	4.727
Lys-161@NZ	UCN-01@C=O	Electrostatic	4.350
Tyr-157	UCN-01	Stacking	4.204
Trp-160	UCN-01	Stacking	2.878

infusion rate, which effectively reduced the administered dose by 50% for the second and subsequent courses. In addition, the time between courses was increased from 2 weeks to 4 weeks (29). The extremely low clearance and small distribution volume of UCN-01 in humans may be partially caused by its high degree of binding to hAGP (32). Whereas many drugs that associate with hAGP have K_a values of 10^5–10^6 M^{-1}, UCN-01 is unique in its high affinity binding to hAGP, and has a K_a value of 8×10^8 M^{-1}. The results of this extraordinarily high binding affinity include a low volume of distribution (which approximates the extracellular volume) and long $t_{1/2}$ (32). The pharmacokinetic effects of the high affinity of UCN-01 for interaction with hAGP indicate that plasma levels of hAGP should be an important consideration in planning of clinical treatment. hAGP has been reported to be a major drug binding plasma protein that interacts mainly with basic drugs (63). Previous studies indicate that hAGP has 1 common drug binding site, which appears to be wide and flexible (61). Characterization of the binding site of UCN-01 on hAGP by Kurata *et al.* (58) revealed partial overlap with amino acid residues implicated in binding of basic drugs, acidic drugs, and steroid hormones. In a previous attempt to further characterize the binding site, we found that Trp-160 is particularly likely to play a major role in the binding of UCN-01. However, because that conclusion was the result of deducing the location of the 3 tryptophan residues, other experimental approaches are needed to confirm it. Currently, no x-ray crystallographic data is available for hAGP, which is a heterogeneous protein consisting of different isoforms and glycosylation states that hinder crystallization. Therefore, in the present study, we examined the possibility of using UCN-01 as a photoaffinity-labeling agent. An ideal photolabeling reagent is stable not only in storage but also under the conditions in which the experiments are performed. Another problem with reagent stability is covalent attachment in the dark, either specific or nonspecific, to the protein under study. All the advantages of photoaffinity labeling are lost if such covalent attachment occurs. In the present study, a covalent bond was formed between UCN-01 and hAGP only upon photoirradiation (Fig. 2).

The results of the present examination of photoinhibition by staurosporine and UCN-02 were as expected (Table I). It is interesting that a change in the configuration of the hydroxyl group of UCN-01 or substitution of a hydrogen atom at the C-7 position of UCN-01 caused a decrease in binding inhibition effects. This confirms our finding that the substituent at C-7 of the UCN-01 molecule governs the affinity of its binding to hAGP. On the other hand, the extensive photoinhibition by progesterone, but not warfarin or propranolol, suggests that the binding site of staurosporine analogs overlaps to a greater extent with the binding site of steroids. This sharing of a binding region between UCN-01 and steroids is thought to be of minimal clinical significance, given the increased hAGP concentration in cancer and the extremely high binding affinity of UCN-01 for hAGP.

Sequence analysis of the major radioactive tryptic peptides separated from hAGP photolabeled with [^{3}H]UCN-01 showed that these peptides correspond to amino acids Ser-153 to Lys-161 of hAGP. In addition, no phenylthiohydantoin (PTH) derivatives were detected at the 8th cycle, which corresponds to the 160th Trp residue (Fig. 7), indicating that the covalent bond formed upon photolabeling of [^{3}H]UCN-01 to hAGP is relatively stable under the conditions of Edman degradation, and that it is highly likely that Trp-160 was photolabeled by [^{3}H]UCN-01.

All naturally occurring genetic variants of hAGP conserve the 3 Trp residues in the protein amino acid sequence: Trp-25, Trp-122, and Trp-160 (64). It is noteworthy that there is no significant difference in the binding percentage of UCN-01 between the F1*S and A variants of hAGP (38). 2 of 3 Trp residues of hAGP are relatively shielded from the bulk solvent, whereas the third Trp residue is located on the periphery of the domain. It has been deduced that Trp-25 is located deep in the binding pocket, and that Trp-122 is located in the central hydrophobic pocket of the protein (65). This suggests that Trp-160 is the Trp residue that is exposed to the bulk solvent. We also used site-directed mutagenesis to identify the key Trp residue involved in UCN-01 binding. Photolabeling of wild-type and mutant rhAGP with [^{3}H]UCN-01 revealed that photoincorporation was significantly lower for W160A than for the wild type. In contrast, the level of photoincorporation observed for the other 2 mutants, W25A and W122A, was comparable to that of the wild type. These results strongly support the hypothesis that Trp-160 is the key amino acid responsible for the extraordinarily high affinity of binding between UCN-01 and hAGP.

Previous studies have revealed the structures of UCN-01 and staurosporine bound to the active conformations of Chk1 (47), phospho-CDK2/cyclin A (66), and PDK1 (67). Coincidentally, as observed in the present study, the most important differences previously observed between staurosporine and UCN-01 complexes are the contacts involving the 7-OH group of UCN-01. Komander *et al.* (67) analyzed the relative affinities of staurosporine and UCN-01 for 29 different kinases, and found that binding that was potently inhibited by UCN-01 tended to involve molecules with a side chain that can directly form a hydrogen bond with the 7-OH group of UCN-01. Taking into account the experimental spectra and the unfavorable docking energy, Zsila *et al.* (68) suggested that it is unlikely that curcumin binds inside the central cavity of hAGP. The present docking models show that UCN-01 can interact with surface clefts of hAGP containing Trp-160. The interacting amino acid residues identified by the present type II model are consistent with results of our previous experimental studies of chemical modifications and protein binding (38), as well as those of

present studies using photoaffinity labeling and site-directed mutagenesis.

In order to further analyze the binding cleft of type II docking model, staurosporine and UCN-02, a stereoisomer of UCN-01 with an α-OH group at the C-7 position, were used to replace UCN-01 at the same position to produce another two docking models (data not shown). In general, all interacting amino acid residues in the two latter models were similar to those of the former, except that the α-OH group at the C-7 position of UCN-02 interacts with COOH group of Glu-132, in contrast to UCN-01 where the C-7 β-OH group interacts with Lys-161. On the other hand, no interaction of any form with the amino acid side chain could be observed for the substituent at C-7 position of staurosporine where hydrogen atom exists. Another amino acid residue that deserved attention was Lys-135 as its distance from the sugar ring of UCN-02 was more than 5 Å, the greatest among the three models.

The following sequence of binding affinity for hAGP has previously been observed: UCN-01 > staurosporine > UCN-02 (38). The aromatic ring of UCN-01 is stacked on Trp-160, and the hydrophobic interaction is strengthened by the electrostatic interaction between the 7-OH group of UCN-01 and Lys-161, which are located on the same side of Trp-160. In contrast, the hydrogen bond between the 7-OH group of UCN-02 and Glu-132, which is located on the opposite side, appears to weaken the hydrophobic interaction, because the ring of UCN-02 has been diverted away from Trp-160. The aromatic ring of staurosporine is not diverted from Trp-160, due to the absence of the 7-OH group. In order to gain deeper insight on the binding mechanism of UCN-01 to hAGP, experiments using Glu-132 and Lys-161 hAGP mutants to examine the role of each mutated amino acid residue in the high affinity binding of UCN-01 is currently underway in our laboratory.

Staurosporine is a natural product derived from fermentation extracts of several bacterial species. Staurosporine was initially identified as a potent inhibitor of PKC, which is a Ca^{2+}- and phospholipid-activated kinase (69). Different isoforms of PKC are activated in response to growth factors that act on receptor tyrosine kinases and 7-transmembrane domain receptors (70). Studies have revealed that staurosporine is a broad-acting kinase inhibitor with little specificity or selectivity for PKC (71). Recently, the staurosporine analog *N*-benzoylstaurosporine (PKC412) has been reported to exhibit strong hAGP binding, and to have unusual pharmacokinetics similar to those of staurosporine, which were not predicted by animal studies (72). PKC412 is the only staurosporine inhibitor of protein kinases other than UCN-01 that has been subjected to a clinical trial. There has been a study of oral administration of PKC412 once daily (73). It is interesting that PKC412 exhibits complex pharmacology resulting from binding to hAGP. Preclinical experiments had shown extensive binding of PKC412 to human plasma proteins, with ~88–98% protein binding, depending on the drug concentration (72). Rates of binding of PKC412 to hAGP were particularly interesting. In the preclinical experiments, the plasma concentrations of PKC412 were higher, and the half-life was longer than predicted from animal studies and single dose kinetics studies with healthy volunteers (72). In contrast to UCN-01, PKC412 was metabolized to 7-hydroxy-PKC412 and an *O*-demethyl-PKC412, both of which also bound to hAGP. The major metabolite had a particularly long half-life (74). It is possible that PKC412 and its metabolite preferentially bind to hAGP *in vivo*, and this may account for the longer than anticipated plasma half-life. The dynamics of dissociation of PKC412 from plasma proteins and tissue distribution of PKC412 are likely to be complex, and plasma levels may not accurately reflect drug concentration in target tissues. Because plasma pharmacokinetic evaluation is complicated by protein binding and metabolism, studies using biologic markers of PKC inhibition can contribute to optimization of PKC412 administration.

CONCLUSIONS

Because of the potential implications of species-specific binding of UCN-01 to hAGP in human plasma for the development of staurosporine analogs, studies of analogs of UCN-01 and of PKC412, which lack hAGP binding or very weakly bind to hAGP, should be conducted along with studies of the potential usefulness of staurosporine pharmacophores. Characterization of the binding site of UCN-01 on hAGP using photoaffinity labeling and site-directed mutagenesis techniques has provided direct evidence that strongly indicates that Trp-160 plays an important role in the binding interaction between UCN-01 and hAGP. In addition to the obvious pharmacokinetic implications of the extraordinarily high affinity of binding of UCN-01 to hAGP, the present results suggest that hAGP is a suitable platform for further design of novel staurosporine analog anticancer drugs, and also for evaluation of side effects and drug interaction in clinical settings. The present results provide clues to the design of future second-generation therapeutic agents, and can serve as a basis for future studies of UCN-01 administered alone and in combination with other anticancer drugs, particularly DNA-damaging agents.

Acknowledgment—We thank Dr. Vladimir Kopecky, Jr. of the Institute of Physics, Charles University in Prague, for providing us with the protein moiety of hAGP in the native state and with docked progesterone in a PDB format.

REFERENCES

1. Schmid, K., Nimerg, R. B., Kimura, A., Yamaguchi, H., and Binette, J. P. (1977) *Biochim. Biophys. Acta* **492,** 291–302
2. Kremer, J. M., Wilting, J., and Janssen, L. H. (1988) *Pharmacol. Rev.* **40,** 1–47
3. Van Dijk, W. (1995) *Adv. Exp. Med. Biol.* **376,** 223–229
4. Hochepied, T., Berger, F. G., Baumann, H., and Libert, C. (2003) *Cytokine Growth Factor Rev.* **14,** 25–34
5. Cheresh, D. A., Haynes, D. H., and Distasio, J. A. (1984) *Immunology* **51,** 541–548
6. Morita, K., and Yamaji, A. (1995) *Ther. Drug Monit.* **17,** 107–112
7. Mackiewicz, A., and Mackiewicz, K. (1995) *Glycoconj. J.* **12,** 241–247
8. Duche, J. C., Urien, S., Simon, N., Malaurie, E., Monnet, I., and Barre, J. (2000) *Clin. Biochem.* **33,** 197–202
9. Fan, C., Stendahl, U., Stjernberg, N., and Beckman, L. (1995) *Oncology* **52,** 498–500
10. Mazoit, J. X., and Dalens, B. J. (2004) *Clin. Pharmacokinet.* **43,** 17–32
11. Veering, B. T., Burm, A. G., Feyen, H. M., Olieman, W. M., Souverijn, J. H., and Van Kleef, J. W. (2002) *Anesthesiology* **96,** 1062–1069
12. Hedaya, M. A., and Daoud, S. S. (2001) *Anticancer Res.* **21,** 4005–4010
13. Gambacorti-Passerini, C., Zucchetti, M., Russo, D., Frapolli, R., Verga, M., Bungaro, S., Tornaghi, L., Rossi, F., Pioltelli, P., Pogliani, E., Alberti, D., Corneo, G., and D'Incalci, M. (2003) *Clin. Cancer Res.* **9,** 625–632
14. Bruno, R., Olivares, R., Berille, J., Chaikin, P., Vivier, N., Hammershaimb, L., Rhodes, G. R., and Rigas, J. R. (2003) *Clin. Cancer Res.* **9,** 1077–1082
15. Takahashi, I., Kobayashi, E., Asano, K., Yoshida, M., and Nakano, H. (1987) *J. Antibiot (Tokyo)* **40,** 1782–1784
16. Penuelas, S., Alemany, C., Noe, V., and Ciudad, C. J. (2003) *Eur. J. Biochem.* **270,** 4809–4822
17. Yu, Q., La, Rose, J., Zhang, H., Takemura, H., Kohn, K. W., and Pommier, Y. (2002) *Cancer Res.* **62,** 5743–5748
18. Facchinetti, M. M., De, Siervi, A., Toskos, D., and Senderowicz, A. M. (2004) *Cancer Res.* **64,** 3629–3637
19. Dai, Y., Pei, X. Y., Rahmani, M., Conrad, D. H., Dent, P., and Grant, S. (2004) *Blood* **103,** 2761–2770
20. Tenzer, A., and Pruschy, M. (2003) *Curr. Med. Chem. Anti-Cancer Agents* **3,** 35–46
21. Akinaga, S., Gomi, K., Morimoto, M., Tamaoki, T., and Okabe, M. (1991) *Cancer Res.* **51,** 4888–4892
22. Akinaga, S., Nomura, K., Gomi, K., and Okabe, M. (1994) *Cancer Chemother. Pharmacol.* **33,** 273–280
23. Seynaeve, C. M., Stetler-Stevenson, M., Sebers, S., Kaur, G., Sausville, E. A., and Worland, P. J. (1993) *Cancer Res.* **53,** 2081–2086
24. Senderowicz, A. M. (2003) *Oncogene* **22,** 6609–6620
25. Akiyama, T., Yoshida, T., Tsujita, T., Shimizu, M., Mizukami, T., Okabe, M., and Akinaga, S. (1997) *Cancer Res.* **57,** 1495–1501
26. Akinaga, S., Nomura, K., Gomi, K., and Okabe, M. (1993) *Cancer Chemother. Pharmacol.* **32,** 183–189
27. Abe, S., Kubota, T., Otani, Y., Furukawa, T., Watanabe, M., Kumai, K., and Kitajima, M. (2000) *Jpn. J. Cancer Res.* **91,** 1192–1198
28. Bunch, R. T., and Eastman, A. (1996) *Clin. Cancer Res.* **2,** 791–797

29. Sausville, E. A., Arbuck, S. G., Messmann, R., Headlee, D., Bauer, K. S., Lush, R. M., Murgo, A., Figg, W. D., Lahusen, T., Jaken, S., Jing, X., Roberge, M., Fuse, E., Kuwabara, T., and Senderowicz, A. M. (2001) *J. Clin. Oncol.* **19,** 2319–2333
30. Senderowicz, A. M. (2002) *Hematol. Oncol. Clin. North Am.* **16,** 1229–1253
31. Fuse, E., Tanii, H., Takai, K., Asanome, K., Kurata, N., Kobayashi, H., Kuwabara, T., Kobayashi, S., and Sugiyama, Y. (1999) *Cancer Res.* **59,** 1054–1060
32. Fuse, E., Tanii, H., Kurata, N., Kobayashi, H., Shimada, Y., Tamura, T., Sasaki, Y., Tanigawara, Y., Lush, R. D., Headlee, D., Figg, W. D., Arbuck, S. G., Senderowicz, A. M., Sausville, E. A., Akinaga, S., Kuwabara, T., and Kobayashi, S. (1998) *Cancer Res.* **58,** 3248–3253
33. Sausville, E. A., Lush, R. D., Headlee, D., Smith, A. C., Figg, W. D., Arbuck, S. G., Senderowicz, A. M., Fuse, E., Tanii, H., Kuwabara, T., and Kobayashi, S. (1998) *Cancer Chemother. Pharmacol.* **42,** 54–59
34. Bailey, D. N., and Briggs, J. R. (2004) *Ther. Drug Monit.* **26,** 40–43
35. Nakai, D., Kumamoto, K., Sakikawa, C., Kosaka, T., and Tokui, T. (2004) *J. Pharm. Sci.* **93,** 847–854
36. Kute, T., and Westphal, U. (1976) *Biochim. Biophys. Acta* **420,** 195–213
37. Haughey, D. B., Steinberg, I., and Lee, M. H. (1985) *J. Pharm. Pharmacol.* **37,** 285–288
38. Katsuki, M., Chuang, V. T. G., Nishi, K., Suenaga, A., and Otagiri, M. (2004) *Pharm. Res.* **21,** 1648–1655
39. Hatanaka, Y., and Sadakane, Y. (2002) *Curr. Top Med. Chem.* **2,** 271–288
40. Chang, S. H., and Low, P. S. (2003) *J. Biol. Chem.* **278,** 6879–6884
41. Sato, T., Shimada, Y., Nagasawa, N., Nakanishi, S., and Jingami, H. (2003) *J. Biol. Chem.* **278,** 4314–4321
42. Nishi, K., Fukunaga, N., and Otagiri, M. (2004) *Drug Metab. Dispos.* **32,** 1069–1074
43. Braman, J., Papworth, C., and Greener, A. (1996) *Methods Mol. Biol.* **57,** 31–44
44. Zor, T., and Selinger, Z. (1996) *Anal. Biochem.* **236,** 302–308
45. Davis, M. T., and Lee, T. D. (1992) *Protein Sci.* **1,** 935–944
46. Kopecky, V, Jr., Ettrich, R., Hofbauerova, K., and Baumruk, V. (2003) *Biochem. Biophys. Res. Commun.* **300,** 41–46
47. Zhao, B., Bower, M. J., McDevitt, P. J., Zhao, H., Davis, S. T., Johanson, K. O., Green, S. M., Concha, N. O., and Zhou, B. B. (2002) *J. Biol. Chem.* **277,** 46609–46615
48. Rarey, M., Kramer, B., Lengauer, T., and Klebe, G. (1996) *J. Mol. Biol.* **261,** 470–489
49. Jones, G., Willett, P., Glen, R. C., Leach, A. R., and Taylor, R. (1997) *J. Mol. Biol.* **267,** 727–748
50. Muegge, I., and Martin, Y. C. (1999) *J. Med. Chem.* **42,** 791–804
51. Kuntz, I. D., Blaney, J. M., Oatley, S. J., Langridge, R., and Ferrin, T. E. (1982) *J. Mol. Biol.* **161,** 269–288
52. Eldridge, M. D., Murray, C. W., Auton, T. R., Paolini, G. V., and Mee, R. P. (1997) *J. Comput-Aided Mol. Design* **11,** 425–445
53. Cornell, W. D., Cieplak, P., Bayly, C. I., Gould, I. R., Merz, K. M., Jr., Ferguson, D. M., Spellmeyer, D. C., Fox, T., Caldwell, J. W., and Kollman, P. A. (1995) *J. Am. Chem. Soc.* **117,** 5179–5197
54. Gasteiger, J., and Marsili, M. (1980) *Tetrahedron* **36,** 3219–3228
55. Gasteiger, J., and Marsili, M. (1981) *Organ. Magn. Reson.* **15,** 353–360
56. Marsili, M., and Gasteiger, J. (1980) *Croat. Chem. Acta* **53,** 601–614
57. Purcell, W. P., and Singer, J. A. (1967) *J. Chem. Eng. Data* **12,** 235–246
58. Kurata, N., Matsushita, S., Nishi, K., Watanabe, H., Kobayashi, S., Suenaga, A., and Otagiri, M. (2000) *Biol. Pharm. Bull.* **23,** 893–895
59. Urien, S., Giroud, Y., Tsai, R. S., Carrupt, P. A., Bree, F., Testa, B., and Tillement, J. P. (1995) *Biochem. J.* **306,** 545–549
60. Israili, Z. H., and Dayton, P. G. (2001) *Drug Metab. Rev.* **33,** 161–235
61. Miyoshi, T., Yamamichi, R., Maruyama, T., Takadate, A., and Otagiri, M. (1992) *Biochem. Pharmacol.* **43,** 2161–2167
62. Taheri, S., Cogswell, L. P., 3rd., Gent, A., and Strichartz, G. R. (2003) *J. Pharmacol. Exp. Ther.* **304,** 71–80
63. Routledge, P. A. (1986) *Br. J. Clin. Pharmacol.* **22,** 499–506
64. Dente, L., Pizza, M. G., Metspalu, A., and Cortese, R. (1987) *EMBO J.* **6,** 2289–2296
65. Friedman, M. L., Schlueter, K. T., Kirley, T. L., and Halsall, H. B. (1985) *Biochem. J.* **232,** 863–867
66. Johnson, L. N., De Moliner, E., Brown, N. R., Song, H., Barford, D., Endicott, J. A., and Noble, M. E. (2002) *Pharmacol. Ther.* **93,** 113–124
67. Komander, D., Kular, G. S., Bain, J., Elliott, M., Alessi, D. R., and Van Aalten, D. M. (2003) *Biochem. J.* **375,** 255–262
68. Zsila, F., Bikadi, Z., and Simonyi, M. (2004) *Bioorg. Med. Chem.* **12,** 3239–3245
69. Tamaoki, T., Nomoto, H., Takahashi, I., Kato, Y., Morimoto, M., and Tomita, F. (1986) *Biochem. Biophys. Res. Commun.* **135,** 397–402
70. Rodriguez-Fernandez, J. L., and Rozengurt, E. (1998) *J. Biol. Chem.* **273,** 19321–19328
71. Katira, A., Knox, K. A., Finney, M., Michell, R. H., Wakelam, M., and Gordon, J. (1993) *Clin. Exp. Immunol.* **92,** 347–352
72. Propper, D. J., McDonald, A. C., Man, A., Thavasu, P., Balkwill, F., Braybrooke, J. P., Caponigro, F., Graf, P., Dutreix, C., Blackie, R., Kaye, S. B., Ganesan, T. S., Talbot, D. C., Harris, A. L., and Twelves, C. (2001) *J. Clin. Oncol.* **19,** 1485–1492
73. Monnerat, C., Henriksson, R., Le, Chevalier, T., Novello, S., Berthaud, P., Faivre, S., and Raymond, E. (2004) *Ann. Oncol.* **15,** 316–323
74. Eder, J. P., Jr., Garcia-Carbonero, R., Clark, J. W., Supko, J. G., Puchalski, T. A., Ryan, D. P., Deluca, P., Wozniak, A., Campbell, A., Rothermel, J., and LoRusso, P. (2004) *Investig. New Drugs* **22,** 139–150

Available online at www.sciencedirect.com
SCIENCE DIRECT
Biochimica et Biophysica Acta 1668 (2005) 145–155
BIOCHIMICA ET BIOPHYSICA ACTA
BBA
http://www.elsevier.com/locate/bba

Antioxidant effect of bovine serum albumin on membrane lipid peroxidation induced by iron chelate and superoxide

Kenji Fukuzawa[a,*], Yasuaki Saitoh[a], Kaori Akai[a], Kentaro Kogure[a], Satoru Ueno[a], Akira Tokumura[a], Masaki Otagiri[b], Akira Shibata[a]

[a]*Graduate School of Pharmaceutical Sciences, The University of Tokushima, Shomachi-1, Tokushima 770-8505, Japan*
[b]*Graduate School of Pharmaceutical Sciences, Kumamoto University, Oe-honmachi-5, Kumamoto 862-0973, Japan*

Received 14 January 2004; accepted 2 December 2004
Available online 24 December 2004

Abstract

Albumin is supposed to be the major antioxidant circulating in blood. This study examined the prevention of membrane lipid peroxidation by bovine serum albumin (BSA). Lipid peroxidation was induced by the exposing of enzymatically generated superoxide radicals to egg yolk phosphatidylcholine liposomes incorporating lipids with different charges in the presence of chelated iron catalysts. We used three kinds of Fe^{3+}-chelates, which initiated reactions that were dependent on membrane charge: Fe^{3+}-EDTA and Fe^{3+}-EGTA catalyzed peroxidation in positively and negatively charged liposomes, respectively, and Fe^{3+}-NTA, a renal carcinogen, catalyzed the reaction in liposomes of either charge. Fe^{3+}-chelates initiated more lipid peroxidation in liposomes with increased zeta potentials, followed by an increase of their availability for the initiation of the reaction at the membrane surface. BSA inhibits lipid peroxidation by preventing the interaction of iron chelate with membranes, followed by a decrease of its availability in a charge-dependent manner depending on the iron-chelate concentration: one is accompanied and the other is unaccompanied by a change in the membrane charge. The inhibitory effect of BSA in the former at high concentrations of iron chelate would be attributed to its electrostatic binding with oppositely charged membranes. The inhibitory effect in the latter at low concentrations of iron chelate would be caused by BSA binding with iron chelates and keeping them away from membrane surface where lipid peroxidation is initiated. Although these results warrant further in vivo investigation, it was concluded that BSA inhibits membrane lipid peroxidation by decreasing the availability of iron for the initiation of membrane lipid peroxidation, in addition to trapping active oxygens and free radicals.

Keywords: Serum albumin; Lipid peroxidation; Superoxide; Liposome; Membrane; Antioxidant; Free radical; Xanthine oxidase; Nitrilotriacetate; Iron

1. Introduction

Reactive oxygen species participate in the development of many pathologic events by causing oxidative deterioration of biological macromolecules such as DNA, proteins, and membrane lipids [1,2]. In particular, oxidation of membranes and lipoprotein lipids in circulation has been implicated in the pathogenesis of many vascular disorders, including atherosclerosis, diabetes, and hypertension [3,4], and there have been extensive studies on the initiation and prevention of lipid peroxidation.

Albumin is considered the major circulating antioxidant in the blood [5–7], which is exposed to continuous oxidative

Abbreviations: BSA, bovine serum albumin; aBSA, acetylated BSA; mBSA, methylated BSA; nBSA, native BSA; DCP, dicetylphosphate; EDTA, ethylenediamine tetraacetic acid; EGTA, bis(2-aminoethyl ether)-ethyleneglycol tetraacetic acid; EYPC, egg yolk phosphatidylcholine; HEPES, 2-hydroxyethylpiperazine-2-ethanesulfonic acid; NTA, nitrilotriacetic acid (nitrilotriacetate); PC-OOH, hydroperoxides of egg yolk phosphatidylcholine; poly-Glu, poly-L-glutamic acid; poly-Lys, poly-L-lysine; poly (Lys-Phe), poly-L-lysine-L-phenylalanine; SA, stearylamine; TBA, thiobarbituric acid; X, xanthine; XO, xanthine oxidase

* Corresponding author. Tel.: +81 88 633 7248; fax: +81 88 633 9572.
E-mail address: fukuzawa@ph.tokushima-u.ac.jp (K. Fukuzawa).

0005-2736/$ - see front matter © 2004 Elsevier B.V. All rights reserved.
doi:10.1016/j.bbamem.2004.12.006

stress. In vitro experiments have shown that serum albumin protects human low-density lipoproteins from copper-mediated oxidation and red blood cells from hemolysis due to free radical membrane damage [8]. Further, it was reported that serum albumin protects cultured cells, such as renal tubular cells, macrophages, aortic endothelial cells, and lung fibroblasts, from oxygen radical damage [9,10]. Albumin protects cells mainly by directly scavenging reactive oxygen species by trapping them. Dean et al. [11] reported that bovine serum albumin (BSA) inhibited membrane lipid peroxidation of liposomes induced by lipid-soluble radicals less than that induced by water-soluble radicals, an effect that is probably due to lower scavenging efficiency for lipid-soluble radicals than for water-soluble radicals.

The superoxide anion radical ($O_2^{\cdot -}$) produced in aerobic organisms is widely held to be a major initiator of biological damage resulting in pathophysiological events associated with a variety of diseases [12,13]. The biological effectiveness of $O_2^{\cdot -}$ is usually explained by the formation of more-reactive species derived from it. A specific example is the oxidation of unsaturated lipids in membranes, an important event in pathophysiology, which cannot be initiated directly by $O_2^{\cdot -}$. The conversion of $O_2^{\cdot -}$ to more reactive intermediates requires the participation of metal catalysts, of which iron is the most important in biological systems [12–15].

Recently, we investigated the membrane lipid peroxidation in liposomes exposed to $O_2^{\cdot -}$ in the presence of chelated iron, and proposed that a Fenton-like reaction of iron-chelate with preformed lipid peroxides at the membrane surface triggers the initiation of lipid hydroperoxide (LOOH) formation [15,16]:

$$Fe^{3+} - \text{chelate} + O_2^{\cdot -} \rightarrow Fe^{2+} - \text{chelate} + O_2 \quad (1)$$

$$Fe^{2+} - \text{chelate} + \text{L} - \text{OOH} \rightarrow Fe^{3+} - \text{chelate} + \text{L} - \text{O}^{\cdot} \quad (2)$$

$$\text{L} - \text{O}^{\cdot} + \text{LH} \rightarrow \text{L} - \text{OH} + \text{L}^{\cdot} \quad (3)$$

$$\text{L}^{\cdot} + O_2 \rightarrow \text{L} - \text{OO}^{\cdot} \quad (4)$$

$$\text{L} - \text{OO}^{\cdot} + \text{LH} \rightarrow \text{L} - \text{OOH} + \text{L}^{\cdot} \quad (5)$$

where LH is the unoxidized lipid and L$^{\cdot}$, L-O$^{\cdot}$, and L-OO$^{\cdot}$; the lipid carbon-centered, alkoxyl, and peroxyl radicals, respectively.

This initiation system seems most likely to occur in blood circulation. Therefore, in this study, we used this lipid peroxidation system and investigated the inhibitory effect of BSA on it from the point of view of obstruction of the Fenton-like reaction that occurs at the membrane surface, and which differs from its well-known antioxidant effect due to trapping active oxygens and free radicals.

2. Materials and methods

2.1. Materials

Egg yolk phosphatidylcholine (EYPC) was obtained from Nippon Oil and Fats (Tokyo, Japan). The fatty acid composition (mol%) of EYPC was 33.1 palmitate, 1.2 palmitoleate, 11.6 stearate, 30.0 oleate, 15.5 linoleate, 3.3 arachidonate, and 5.3 docosahexaenoate. The commercial EYPC sample was contaminated with 0.3–0.4 mol% of hydroperoxide, as determined by the ferric–xylenol orange method [17]. Bovine serum albumin, fatty acid-free (native BSA:nBSA), carboxymethylated BSA (mBSA), xanthine oxidase (XO), stearyl amine (SA), dicetylphosphate (DCP), poly-L-lysine (poly-Lys) (m.w., 48100), poly-L-glutamic acid (poly-Glu) (m.w.,72500), and poly-L-lysine-L-phenylalanine (1:1) (poly (Lys-Phe)) (m.w., 35400) were purchased from Sigma Chemical (St. Louis, MO). Sodium ethylenediamine tetraacetate (EDTA-2Na), bis (2-aminoethyl ether) ethyleneglycol tetraacetic acid (EGTA), 2-hydroxyethylpiperazine-2-ethanesulfonic acid (HEPES), xylenol orange, and $Fe(NO_3)_3$ were obtained from Wako Pure Chemical Industries (Tokyo, Japan). Sodium nitrilotriacetate (NTA-2Na) and $FeSO_4$ were from Nacalai Tesque (Kyoto, Japan). All other reagents were of analytical grade. Acetylated BSA (aBSA) was prepared using a modification of the method of Basu et al. [18].

2.2. Preparation of liposomes

Liposomes were prepared as described previously [15]. Stock solutions of EYPC in chloroform with or without DCP or SA were evaporated under nitrogen. The resulting thin lipid films were dispersed in 10 mM HEPES buffer, pH 7.4, in a vortex mixer and subjected to ultrasonic irradiation in a Bransonic-12 sonic bath (Yamato Tokyo, Japan) at 40 °C for 5 min (charged liposomes) or 10 min (uncharged liposomes). When required, the EYPC was freed from contaminating hydroperoxides of EYPC (PC-OOH) by treatment with triphenylphosphine (TPP) [19] in chloroform just before the preparation of liposomes.

2.3. BSA acetylation and characterization of BSAs

nBSA was acetylated using acetic anhydride [18]. To 3 ml of 0.15 M NaCl solution of nBSA (15 mg/ml), 3 ml of sodium acetate-saturated solution was added, and then 40 μl of acetic anhydride was slowly added (2 μl/3 min) at room temperature. After incubation for 30 min, acetylated BSA was dialyzed using a hydrated dialysis membrane (Wako Chem., USA) at 4 °C in 0.15 M NaCl for 24 h and further in 10 mM HEPES buffer solution (pH 7.4) for 3 h. The protein concentration of the BSA preparation was determined using the Lowry method [20]. The net charge of the albumins was investigated by determining their migration times in capillary electrophoresis [21]. The migration times for

aBSA was 12.71±0.10 min (S.D., n=3), which was slightly but significantly long as compared with that of nBSA (12.21±0.02 min), indicating additional net negative charge. The amounts of carbonyl groups measured according to the dinitrophenylhydrazine method [22] were 119% higher in aBSA (0.166 mol carbonyl/mol BSA) than that in nBSA (0.139 mol carbonyl/mol BSA). Purchased mBSA prepared by Mandel and Hershey [23] was well confirmed as a net positively charged basic protein [24].

2.4. Assays of lipid peroxidation

Lipid peroxidation of EYPC liposomes was measured by following oxygen consumption [16]. The following conditions were used for Fe^{3+}-chelate-dependent lipid peroxidation initiated by $O_2^{\cdot-}$ in liposomes. The test systems consisted of liposomes containing 1 mM EYPC with or without DCP or SA in 3.6 ml of 10 mM HEPES buffer pH 7.4 at 37 °C. The oxidation was started by the addition of 10 μl Fe^{3+}-chelate (final concentrations 30 μM Fe^{3+} and 33 μM chelator), 10 μl xanthine (30 μM), and finally 10 μl XO (1 mU/ml) to 3.6 ml of liposome suspensions in 10 mM HEPES buffer (pH 7.4). The Fe^{3+}-chelates were prepared by mixing $Fe(NO_3)_3$ in H_2O or dilute HCl solution with the chelator (1.0 to 1.1 molar ratio). The rate of oxygen consumption associated with lipid peroxidation was measured with a Clark-type oxygen electrode, assuming an oxygen concentration of 217 nmol/ml in the initial incubation mixture at 37 °C.

The generation of $O_2^{\cdot-}$ in human granulocytes from normal blood samples during phagocytosis was reported to be 5–30 mU XO equivalent/ml [25]. In this study, the XO content (1 mU XO/ml) was decided considering the suitable condition for measurement of lipid peroxidation, under which O_2 consumption due to $O_2^{\cdot-}$ generation is negligible in comparison with that due to lipid peroxidation. The rate of $O_2^{\cdot-}$ generation by 1 mU XO/ml used in this experiment is equivalent to the rate (1 μM $O_2^{\cdot-}$/min) observed in our previous study that $O_2^{\cdot-}$ was responsible for apoptosis in rat vascular smooth muscle cells [26]. The thiobarbituric acid (TBA) method was used as described previously [16] to provide another assay for lipid peroxidation. The amount of TBA-reactive substances (TBARS) formed was expressed as equivalents of malondialdehyde (MDA). Other experimental details are described in figure legends.

2.5. Assay of binding of Fe^{3+}-NTA to BSA

Equilibrium dialysis experiments were performed with an Equilibrium Dialyzer (Sanplatec, Osaka, Japan) using a total volume of 13 ml of cells. A hydrated dialysis membrane was washed in deionized water and dried with N_2 gas. To one side of the membrane was added 7 ml of dialysate solution (50 mM HEPES–Tris in 10 mM NaCl buffer, pH 7.4) containing a certain concentration of Fe^{3+}-NTA solution. On the other side of the membrane, 7 ml of the sample (BSA or polypeptide) solution was dialyzed for 24 h. The volumes of the solutions on either side of the membrane were kept constant during the dialysis procedure. Aliquots from the chamber were removed and then free concentrations of Fe^{3+}-NTA were determined by the ferric–xylenol orange method [27]. The percentage binding of Fe^{3+}-NTA to the sample was calculated using the following equation:

$$B\ (\%) = (Abs_a - Abs_b)/Abs_a \times 100$$

where B (%) is the percentage of the added Fe^{3+}-NTA bound to the sample, and Abs_b and Abs_a are the absorbances at 560 nm of Fe^{3+}-NTA in the dialyzed solution with and without a sample, respectively.

2.6. Measurement of zeta potential of liposome membranes

The zeta potentials of the liposomes (1 mM EYPC with or without 0–0.2 mM DCP or SA) in 10 mM HEPES/10 mM NaCl buffer at pH 7.4 were measured electrophoretically in a NICOMP (model 380 apparatus, Particle Sizing Systems, Santa Barbara, California) at room temperature.

3. Results

Preliminary experiments showed that the complete system, made up of liposomes formed from 1 mM EYPC supplemented with 0.2 mM SA or 0.1 mM DCP, 10 mM HEPES buffer at pH 7.4, 1 mU/ml XO, 30 μM X, and Fe^{3+}-NTA (30 μM Fe^{3+}, 33 μM NTA), rapidly consumed oxygen, indicating the occurrence of lipid peroxidation (solid lines (1) in Fig. 1). Oxygen was not consumed if XO was excluded, but slightly consumed if Fe^{3+}-NTA was excluded, possibly due to the generation of $O_2^{\cdot}$ from oxygen by X-XO (broken lines in Fig. 1 (left)), indicating that lipid peroxidation was not induced directly by either $O_2^{\cdot-}$ or Fe^{3+}-NTA. The involvement $O_2^{\cdot-}$ in this process was confirmed by the complete inhibition of oxygen uptake by the addition of superoxide dismutase (100 U/ml) (data not shown). Similarly, oxygen consumption was completely inhibited if liposomes were prepared from EYPC pretreated with triphenylphosphine (TPP) (broken line (1) in Fig. 1 (right)), which reduces endogenous EYPC hydroperoxides (PC-OOH) to the corresponding alcohols (PC-OH) [19], indicating that the presence of PC-OOH was a prerequisite for the induction of lipid peroxidation.

Lines (2)–(4) in Fig. 1 show the time course of Fe^{3+}-NTA/X-XO-dependent lipid peroxidation in liposomes with positive and negative charges in the presence of various BSAs. Three types of BSAs, nBSA with a small net negative charge, negatively charged aBSA, and positively charged mBSA, were used. All BSAs inhibited the lipid peroxidation. The orders of their inhibitory effects were: aBSA>nBSA>mBSA in positively charged SA-EYPC liposomes, and mBSA>nBSA>aBSA in negatively

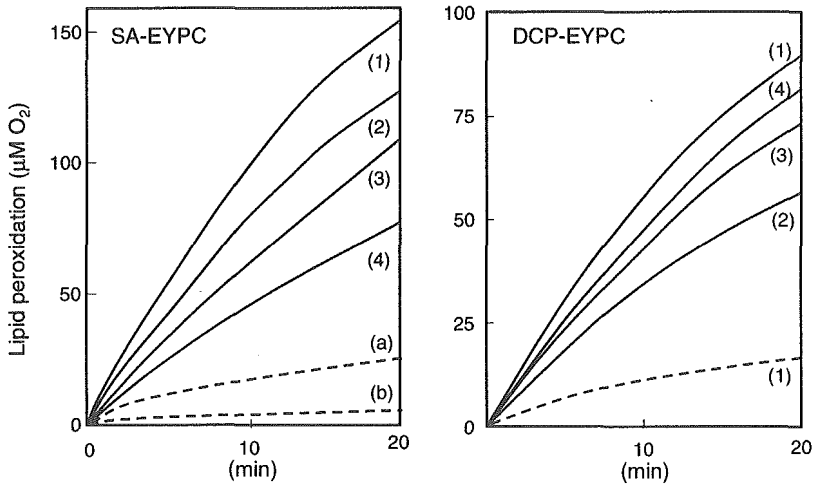

Fig. 1. Inhibition by BSAs of Fe^{3+}-NTA/X-XO-dependent lipid peroxidation in DCP-EYPC and SA-EYPC liposomes. (1) Control; (2) +mBSA; (3) +nBSA; (4) +aBSA. Broken lines in SA-EYPC liposome system indicate the oxygen consumption in the system that excluded only (a) Fe^{3+}-NTA or (b) X-XO from the control system (line (1)). The system of broken line (1) in DCP-EYPC liposome system is all the same to the control system (solid line (1)) but EYPC was pretreated with TPP before the preparation of liposomes. The concentration of BSAs added to the control system was 1.0 mg/ml. Concentrations of reagents in the control system were: 1 mM EYPC, 0.1 mM DCP or 0.2 mM SA, 10 mM HEPES buffer, pH 7.4, 1 mU/ml xanthine oxidase (XO), 30 μM xanthine (X), and iron chelate formed from 30 μM $Fe(NO_3)_3$ and 33 μM NTA. Incubation was at 37 °C, and the reaction started by the addition of XO.

charged DCP-EYPC liposomes. Same orders were observed by the assay of TBARS values (data not shown). Furthermore, nBSA more strongly inhibited TBARS formation in SA-EYPC liposomes (63% inhibition) than in DCP-EYPC liposomes (28% inhibition). These results indicate that the inhibitory effect of BSAs is higher in oppositely charged membranes.

Fe^{3+}-NTA, a renal carcinogen, has been reported to cause apoptosis associated with increase of lipid peroxide and 8-hydroxydeoxyguanosine levels in vivo [28,29] and in vitro [30]. In cultured cells treated with 20–100 μM Fe^{3+}-NTA, oxidative damage [31] and apoptotic [30], cytotoxic [32], and mutagenic [33] effects were observed. Therefore, we used 10–60μM Fe-NTA and examined its concentration dependency for the induction of X-XO-dependent lipid peroxidation in EYPC liposomes containing different amounts of positively charged SA (Fig. 2). The rate of lipid peroxidation increased with an increase in Fe^{3+}-NTA concentration. A decrease of the membranous SA concentration in EYPC liposomes lowered the rate of lipid peroxidation. The addition of nBSA (1 mg/ml) to SA-EYPC (0.2 mM/1 mM EYPC) liposomes slowed down the lipid peroxidation rate. The change in the lipid peroxidation rate in the presence of nBSA was similar to that of the rate depending on the reduction of SA concentration at concentrations of Fe^{3+}-NTA higher than 20 μM. On the contrary, the rate change was quite different from that at concentrations of Fe^{3+}-NTA lower than 10 μM, and the addition of nBSA almost completely inhibited the lipid peroxidation.

Before the antioxidant effect of BSA on the Fe^{3+}-chelate/$O_2^{\cdot-}$-dependent membrane lipid peroxidation at the membrane surface was examined in detail, we investigated the role of Fe^{3+}-chelate at the membrane surface, where a Fenton-like reaction initiates lipid peroxidation. The concentration of Fe^{3+}-chelate chosen was 30 μM, which was suitable for the investigation of inhibiting effect of BSA.

Fig. 3 shows the effect of the membrane charge on the rate of O_2 consumption indicative of lipid peroxidation by Fe^{3+}-chelates (Fe^{3+}-NTA, Fe^{3+}-EGTA, and Fe^{3+}-EDTA). Fe^{3+}-NTA catalyzed the lipid peroxidation both in positively

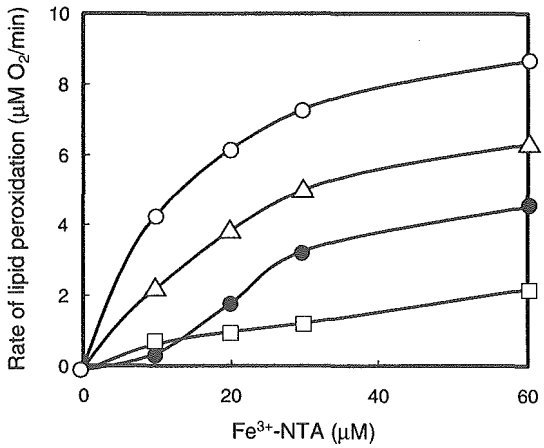

Fig. 2. Inhibitory effect of nBSA on the rate of Fe^{3+}-NTA/X-XO-dependent lipid peroxidation in the presence of various concentrations of Fe^{3+}-NTA in EYPC liposomes containing different amounts of SA. (○) SA-EYPC (0.2 mM/1.0 mM) liposomes; (△) SA-EYPC (0.05 mM/1.0 mM) liposomes; (□) EYPC (1.0 mM) liposomes; (●) SA-EYPC (0.2 mM/1.0 mM) liposomes+nBSA (1.0 mg/ml). The rate in each system was obtained after the subtraction of the value of blank, which was the system that only omitted Fe^{3+}-NTA from the control system.

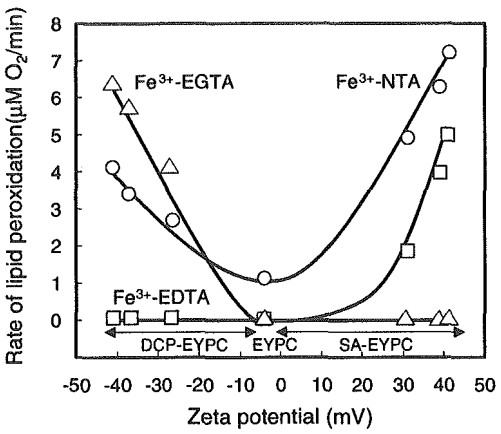

Fig. 3. Rates of Fe^{3+}-chelate/X-XO-dependent oxygen consumption indicative of lipid peroxidation in liposomes with various membrane charges. (○) Fe^{3+}-NTA; (△) Fe^{3+}-EGTA; (□) Fe^{3+}-EDTA. Liposomes were prepared from EYPC containing different amounts of DCP or SA. Concentrations of reagents for lipid peroxidation were: 1 mM EYPC, 0–0.2 mM DCP or SA, 10 mM HEPES buffer, pH 7.4, 1 mU/ml xanthine oxidase (XO), 30 μM xanthine (X), and iron chelate formed from 30 μM $Fe(NO_3)_3$ and 33 μM NTA, EDTA, or EGTA. Incubation was at 37 °C, and the reaction started by the addition of XO.

charged SA-EYPC liposomes and negatively charged DCP-EYPC liposomes, and the rates of lipid peroxidation increased with an increase in the zeta potential of liposomes. Our previous work revealed that the binding of Fe^{3+}-chelates with liposomes is indispensable for the initiation of $O_2^{\cdot-}$ driven lipid peroxidation [16]. Because of the good correlations between the abilities of Fe^{3+}-chelates to induce lipid peroxidation and electrostatic binding to membranes, we supposed that the increase of negative and positive zeta potentials of membranes causes more binding of Fe^{3+}-NTA to membranes, increasing its facilitating effect on lipid peroxidation. The initiation of lipid peroxidation by Fe^{3+}-EGTA and Fe^{3+}-EDTA was also dependent on the zeta potentials of the liposome membranes. The former and the latter catalyzed the lipid peroxidation in negatively charged DCP-EYPC liposomes and positively charged SA-EYPC liposomes, respectively, indicating that membrane charges of DCP-EYPC liposomes and SA-EYPC liposomes are closely associated with the electrostatic binding ability of oppositely charged Fe^{3+}-chelates, such as net positively charged Fe^{3+}-EGTA and net negatively charged Fe^{3+}-EDTA. Increased amounts of Fe^{3+}-chelates bound to the membrane would result in an increase of the availability of the Fe^{3+}-chelates required to initiate lipid peroxidation at the membrane surface.

As shown in Fig. 1, the inhibitory effect of BSA depending on membrane charge was suggested to be due to the neutralization of the membrane charge by electrostatic interaction with the membranes. Thus, we chose systems in which the charges of liposomal membranes and BSAs were opposite, and investigated the correlation between the effects of BSAs on the zeta potentials of liposomes and the rates of Fe^{3+}-NTA/X-XO-dependent lipid peroxidation. The rate of lipid peroxidation was obtained from the initial gradient of the curve in Fig. 1. As shown in Fig. 4, the rates of Fe^{3+}-NTA-dependent lipid peroxidation as a function of BSA concentration were well correlated to the changes in the zeta potentials of liposomes.

To determine the details of the ability of BSA to change the zeta potentials and lipid peroxidation, we compared the rates of lipid peroxidation in liposomes with same zeta potentials, which depend on the concentrations of BSAs added to the membranes and of charged molecules removed from the membranes. The rate of Fe^{3+}-NTA/X-XO-dependent lipid peroxidation in liposomes with different charges was plotted as a function of zeta potential of liposomes in the presence and absence of BSAs (Fig. 5). Under the same zeta potential conditions in systems in which the charge of the liposomes is opposite to that of the BSAs added, the rates of Fe^{3+}-NTA/X-XO-dependent lipid peroxidation were

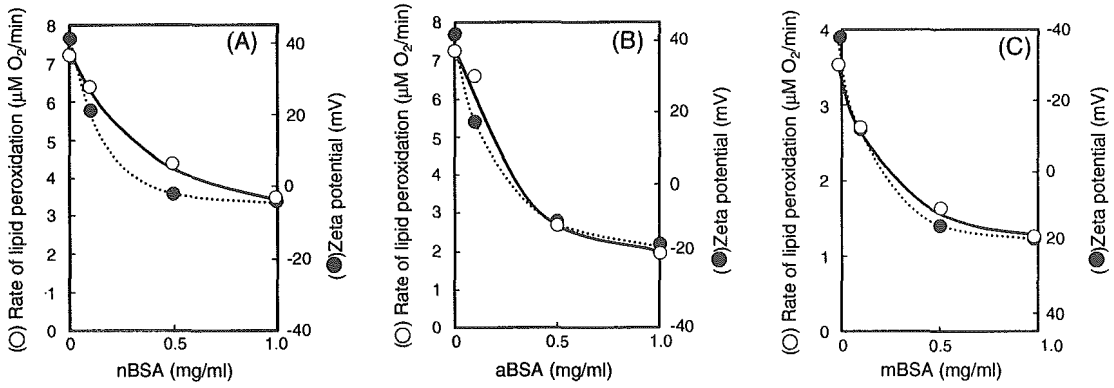

Fig. 4. The effects of the concentration of BSAs on the rate of Fe^{3+}-NTA/X-XO-dependent lipid peroxidation and the zeta potential of EYPC liposomes with DCP or SA. Panel A: nBSA in SA-EYPC liposomes; panel B: aBSA in SA-EYPC liposomes; panel C: mBSA in DCP-EYPC liposomes. (○) Lipid peroxidation; (●) zeta potential. Concentrations of BSAs added to the DCP-EYPC (0.1 mM/1.0 mM) or SA-EYPC (0.2 mM/1.0 mM) liposomes were 0.1 mg/ml–1.0 mg/ml. Other experimental conditions were as shown in Fig. 3.

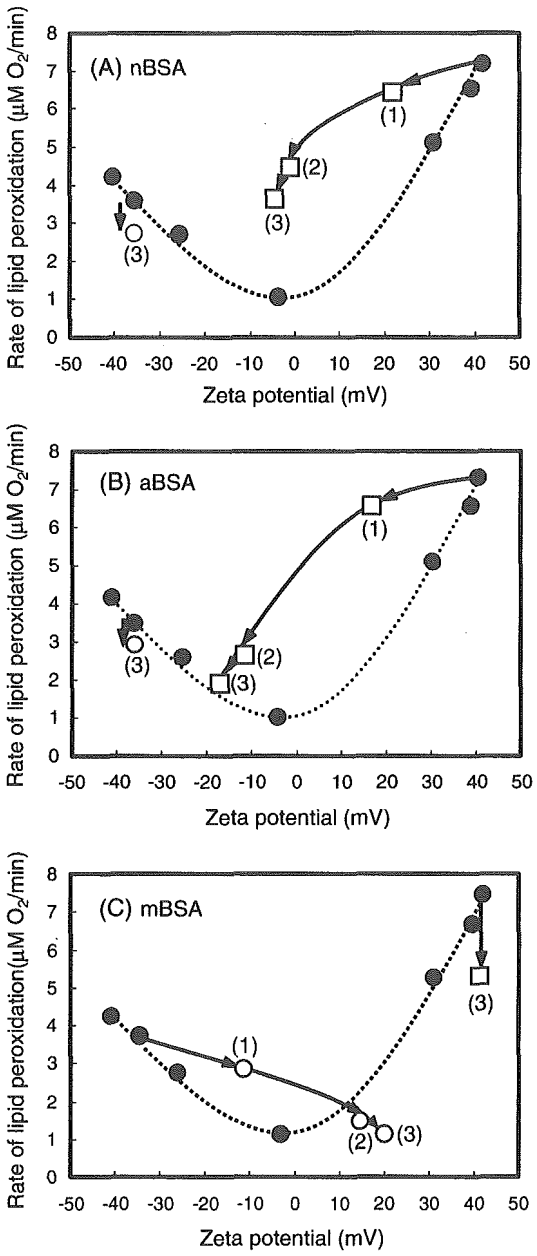

Fig. 5. The rate of Fe^{3+}-NTA/X-XO-dependent lipid peroxidation as a function of zeta potential of liposomes with different charges in the presence or absence of nBSA, aBSA, or mBSA. Panel A: nBSA; panel B: aBSA; panel C: mBSA. (○) DCP-EYPC (0.1 mM/1.0 mM) liposomes in the presence of BSAs; (□) SA-EYPC (0.2 mM/1.0 mM) liposomes in the presence of BSAs; (●) DCP-EYPC (0–0.2 mM/1.0 mM) and SA-EYPC (0–0.2 mM/1.0 mM) liposomes in the absence of BSAs. The concentrations of BSAs added to the liposomes are indicated by numbers: (1) 0.1 mg/ml; (2) 0.5 mg/ml; (3) 1.0 mg/ml. Experimental conditions were as shown in Fig. 3.

always higher in the presence of BSAs (□ in Fig. 5(A) and (B), ○ (1) in Fig. 5(C)) than in their absence (dotted lines in Fig. 5), except for the results shown in Fig. 5(C) (○ (2) and ○ (3)). The reductions of the rate of lipid peroxidation were larger for the addition of aBSA with a high net negative charge (□ in Fig. 5 (B)) than for addition of nBSA with a low net negative charge in SA-EYPC (0.2 mM/1 mM) liposomes (□ in Fig. 5(A)).

On the contrary, in the systems in which BSA was added to identically charged liposomes, Fe^{3+}-NTA/X-XO-dependent lipid peroxidation was inhibited without affecting the zeta potential: nBSA and aBSA with a net negative charge did not affect the zeta potential but weakly inhibited the lipid peroxidation in negatively charged DCP-EYPC (0.1 mM/1 mM) liposomes (○ (3), as shown in Fig. 5(A) and (B)), and mBSA with a net positive charge did not affect the zeta potential but did lower the rate of lipid peroxidation in positively charged SA-EYPC liposomes (□ (3) in Fig. 5(C)).

Fig. 6 shows the effects of mBSA and aBSA on the zeta potentials of liposomes and the rates of Fe^{3+}-EGTA/X-XO-dependent lipid peroxidation. The addition of mBSA lowered both the negative value of the zeta potential and lipid peroxidation in DCP-EYPC liposomes, and their mBSA concentration-dependent decreases correlated well (Fig. 6 (A)). At the same zeta potential, the rates of lipid peroxidation in DCP-EYPC liposomes in the presence of mBSA (○ in Fig. 6 (B)) were always higher than those in their absence (dotted line in Fig. 6 (B)). Furthermore, Fe^{3+}-EGTA/X-XO-dependent lipid peroxidation was not induced in positively charged SA-EYPC liposomes (□ (1) in Fig. 6 (B)) but was induced in DCP-EYPC liposomes with a net positive charge by the addition of a high concentration of mBSA (0.5 mg, 1.0 mg/ml) (○ (3),○ (4) in Fig. 6(B)). On the contrary, Fe^{3+}-EGTA/X-XO-dependent lipid peroxidation was induced in negatively charged DCP-EYPC liposomes (dotted line in Fig. 6(B)) but was not induced in SA-EYPC liposomes with a net negative charge by the addition of a high concentration of aBSA (1.0 mg/ml) (□ (5) in Fig. 6(B)).

Fig. 7 shows the effects of aBSA and mBSA on the zeta potentials of liposomes and the rates of Fe^{3+}-EDTA/X-XO-dependent lipid peroxidation. The addition of aBSA also concentration-dependently neutralized the charge of liposome membranes and lowered the lipid peroxidation rate in SA-EYPC liposomes (Fig. 7 (A)). However, in SA-EYPC liposomes, the rates of lipid peroxidation were always higher in the presence of aBSA (□ in Fig. 7(B)) than in the absence of it (dotted line) at the same zeta potential (Fig. 7 (B)). Fe^{3+}-EDTA/X-XO-dependent lipid peroxidation was not induced in negatively charged DCP-EYPC liposomes (○ (1) in Fig. 7(B)) but was induced in SA-EYPC liposomes with a net negative charge by the addition of a high concentration of aBSA (0.5 mg, 1.0 mg/ml) (□ (3), □ (4) in Fig. 7(B)). On the contrary, Fe^{3+}-EDTA/X-XO-dependent lipid peroxidation was induced in positively charged SA-EYPC liposomes (dotted line in Fig. 7(B)) but was not induced in DCP-EYPC liposomes with a net positive charge by

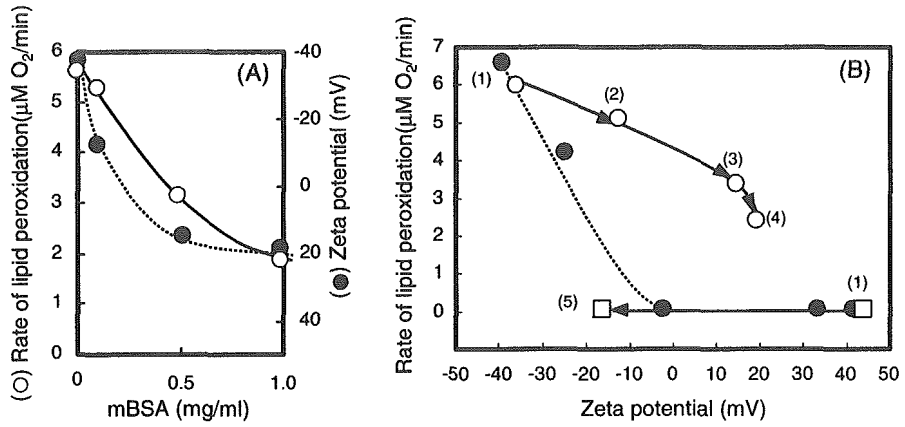

Fig. 6. The effects of the concentration of BSAs on the rate of Fe^{3+}-EGTA/X-XO-dependent lipid peroxidation and the zeta potential of EYPC liposomes with DCP or SA. Panel A: (○) lipid peroxidation; (●) zeta potential. Concentrations of mBSA added to the SA-EYPC (0.2 mM/1.0 mM) liposomes were 0.1–1.0 mg/ml. Panel B: (○) DCP-EYPC (0.1 mM/1.0 mM) liposomes in the presence of BSAs; (□) SA-EYPC (0.2 mM/1.0 mM) liposomes in the presence of BSAs; (●) DCP-EYPC or SA-EYPC liposomes in the absence of BSA. (1) control (no BSA); (2) 0.1 mg mBSA/ml; (3) 0.5 mg mBSA/ml; (4) 1.0 mg mBSA/ml; (5) 1.0 mg aBSA/ml. Other experimental conditions were as shown in Fig. 3.

the addition of a high concentration of mBSA (1.0 mg/ml) (○ (5) in Fig. 7(B)).

The effects of polypeptides, which were used instead of positively charged mBSA and negatively charged aBSA to simplify the experimental system, on the zeta potentials and the rates of lipid peroxidation were investigated further. As shown in Fig. 8(A), the addition of positively charged poly-Lys inhibited Fe^{3+}-EGTA/X-XO-dependent lipid peroxidation in DCP-EYPC liposomes (△), and the addition of negatively charged poly-Glu inhibited Fe^{3+}-EDTA/X-XO-dependent lipid peroxidation in SA-EYPC liposomes (□). Fe^{3+}-EGTA/X-XO-dependent lipid peroxidation was not induced in positively charged SA-EYPC liposomes (dotted line) but was induced in DCP-EYPC liposomes with a net positive charge by the addition of poly-Lys (△). Similarly, Fe^{3+}-EDTA/X-XO-dependent lipid peroxidation was not induced in negatively charged DCP-EYPC liposomes (dotted line) but was induced in SA-EYPC liposomes with a net negative charge by the addition of poly-Glu (□). Thus, the inhibition of lipid peroxidation by polypeptides as well as by BSAs with charges opposite those of the membrane was associated with neutralization of the membrane charge.

We further investigated the effects of positively charged copolypeptides with a hydrophobic residue, poly (Lys-Phe), on the zeta potentials and the rates of Fe^{3+}-NTA/X-XO-dependent lipid peroxidation in EYPC and DCP-EYPC liposomes. As shown in Fig. 8(B), poly (Lys-Phe) behaved similarly to the charged molecule SA in the membranes, and

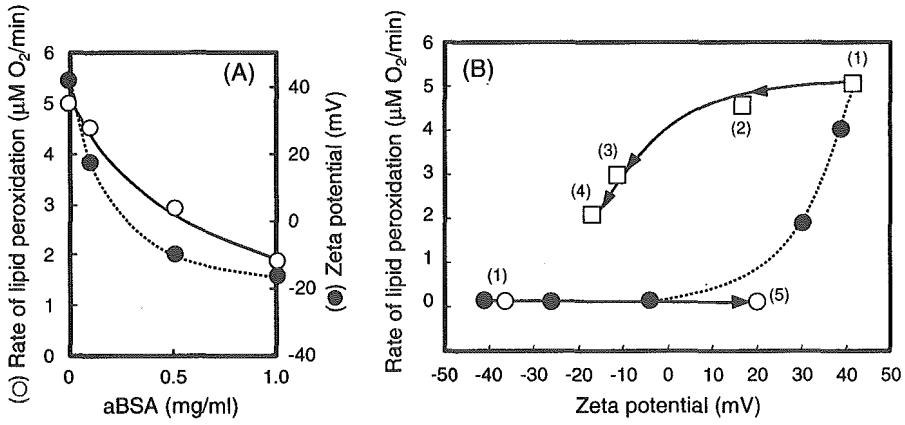

Fig. 7. The effects of the concentration of BSAs on the rate of Fe^{3+}-EDTA/X-XO-dependent lipid peroxidation and the zeta potentials of EYPC liposomes with DCP or SA. Panel A: (○) lipid peroxidation; (●) zeta potential. Concentrations of aBSA added to DCP-EYPC (0.1 mM/1.0 mM) liposomes were 0.1–1.0 mg/ml. Panel B: (○) DCP-EYPC (0.1 mM/1.0 mM) liposomes in the presence of BSAs; (□) SA-EYPC (0.2 mM/1.0 mM) liposomes in the presence of BSAs; (●) DCP-EYPC and SA-EYPC liposomes in the absence of BSAs. (1) control (no BSA); (2) 0.1 mg aBSA/ml; (3) 0.5 mg aBSA/ml; (4) 1.0 mg aBSA/ml; (5) 1.0 mg mBSA/ml. Other experimental conditions were as shown in Fig. 3.